Mössbauer Spectroscopy in Heterogeneous Catalysis

J.M.M. Millet

Mössbauer Spectroscopy in Heterogeneous Catalysis

JEAN-MARC M. MILLET

Institut de Recherches sur la Catalyse et l'Environnement de Lyon, IRCELYON, UMR 5256 CNRS-Université Claude-Bernard, Lyon 1, 2 avenue A. Einstein, F-69626 Villeurbanne Cedex, France; E-mail: jean-marc.millet@ircelyon.univ-lyon1.fr

Mössbauer spectroscopy dates back to 1958 and for characterization of a solid catalyst was first used in 1971; the technique achieved a high point in the 1980s and has been applied only modestly for catalyst characterization since then. The declining use of the technique may be related to the experimental difficulties and the complexity of the spectral analysis. However, the adaptability of Mössbauer spectroscopy to the investigation of catalysts under working conditions and the progress made in the field are evidently leading to a reawakening of interest in its application in catalysis. The value of Mössbauer spectroscopy in catalyst characterization is illustrated by results of investigation of Fischer–Tropsch catalysts by ^{57}Co Mössbauer emission spectroscopy performed at temperatures up to 723 K and pressures up to 40 bar corresponding to industrial working conditions. Furthermore, synchrotron Mössbauer techniques have reached a level of maturity that today allow their use for applications from which catalysts characterization would benefit. This review includes a brief summary of the technique and an overview of applications in catalysis. The majority of investigations have dealt with the isotopes ^{57}Fe, ^{119}Sn, and ^{57}Co (in emission mode). In contrast, investigations focusing on other isotopes, such as ^{197}Au, ^{121}Sb, ^{125}Te, ^{193}Ir, or ^{99}Ru, have been limited in number but very fruitful. Opportunities for future applications to working catalysts are presented and discussed. New techniques related to the use of synchrotron radiation as energy source are emphasized. Such techniques have been applied to isotopes other than ^{57}Fe, such as ^{169}Tm, ^{119}Sn, ^{83}Kr, ^{181}Ta, ^{151}Eu, ^{161}Dy, and ^{149}Sm. The investigation of isotopes such as ^{197}Au, ^{197}Pt, ^{61}Ni, ^{186}W, ^{99}Ru, and ^{99}Rh, is also possible and should strongly benefit catalyst characterization. An effort has been made here to present the techniques, results, and developments in a didactic manner.

Abbreviations: ADC, analog-to-digital converter; CEMS, conversion electron Mössbauer spectroscopy; DCEMS, depth selective conversion electron Mössbauer spectroscopy; DFT, density functional theory; EMS, emission Mössbauer spectroscopy; ESRF, European synchrotron radiation facility; FeZSM-5, iron-containing Zeolite Society Mobil constructed from five-membered-ring building units; GC, gas chromatography; HTP, high throughput; IMS, imaging Mössbauer spectroscopy; MCM-41, mobil composite material/mesoporous composite materials of type 41; MERDJ, *Mössbauer Effect Reference and Data Journal*; NBD, nuclear Bragg diffraction of synchrotron radiation; NFS, nuclear forward scattering of synchrotron radiation; NIS, nuclear inelastic scattering of synchrotron radiation; NQES, nuclear quasi-elastic scattering of synchrotron radiation; NR, nuclear reflectometry of synchrotron radiation; NRS, nuclear resonance scattering; NSAS, small-angle scattering of synchrotron radiation; SCA, single channel analyzer; SOD, second-order Doppler shift; XANES, X-ray absorption near edge spectroscopy; ZSM-5, Zeolite Society Mobil constructed from five-membered-ring building units.

I. Introduction

The nature and breadth of the physical techniques used to investigate solid catalysts continue to increase rapidly in complexity. This statement pertains specifically to Mössbauer spectroscopy, which was applied to the characterization of solid catalysts as early as 1971 (*1*). A retrospective analysis of the use of Mössbauer spectroscopy in catalysis showed that it has consistently accounted for 3–10% of the communications presented at the International Congresses on Catalysis (ICC) (7%t at the ICC in Paris in 2004). Such continuity over the years reflects the high value of this technique in catalyst characterization.

The theoretical basis of Mössbauer spectroscopy as well as its applications to catalyst characterization was reviewed in *Advances in Catalysis* in 1989 (*2*). This thorough article summarizes the physical basis of the technique and significant contributions to the characterization of solid catalysts. Since 1989, Mössbauer spectroscopy has not underwent major developments, and its applications to catalysis have been largely limited to catalysts that were not in reactive atmospheres, notwithstanding the impressive advances that have been made with other techniques in characterizing catalysts under working conditions.

Because this volume is focused on characterization of working catalysts, this chapter is short, including a brief summary of the technique and the underlying physical principles, with a focus on its potential and limitations for investigation of catalysts as they function. Only the essential aspects necessary to understand the technique are presented here. The summary of recent applications emphasizes investigations with less commonly used isotopes and on investigations of catalysts at temperatures and pressures relevant to catalytic reactions. The practical aspects of the use of Mössbauer spectroscopy are not treated in detail, and only a few examples are discussed. Readers searching for more complete reviews of research done using Mössbauer spectroscopy should consult the reviews published in recent years (*3–6*). This article concludes with an evaluation of potential innovations that may arise in the near future and that have not yet been applied for investigations of heterogeneous catalysis.

II. Mössbauer Spectroscopy

A. Physical Principles and Current Capabilities

Mössbauer spectroscopy provides measurements of the resonant absorption of γ-rays by nuclear transitions from a ground state to an excited state. Like other nuclear techniques, it is based on a phenomenon that is specific to a given isotope and for which no interference from other isotopes is possible.

In conventional Mössbauer spectroscopy, X-rays with energies corresponding to nuclear transitions (5–150 keV) can be produced only by use of radioactive sources containing a parent isotope of the absorbing nucleus in an appropriate excited state from which it decays into the ground state with emission of a γ-quantum. For spectroscopic applications, the γ-radiation must be variable. The chemical perturbations

at the nuclear levels are very small relative to the transition energy (i.e., 10^{-8}–10^{-11}). Variations of the energy of the parent radiation of this order of magnitude can be achieved by the Doppler effect. For this purpose the radiation source has to be moved linearly at a low velocity v (generally few mm/s) that will allow variation of the incident energy E_0:

$$E = E_0\left(1 \pm \frac{v}{c}\right). \tag{1}$$

Experimentally, the most convenient way to achieve such movement is to fix the source on a constant-acceleration oscillator allowing imposition of velocities in positive and negative direction depending on whether the source moves toward or away from the absorber: $E = E_0\ (1 \pm v/c)$ (Fig. 1). For convenience, Mössbauer spectrum is taken to correspond to the plot of the intensity of the transmitted or diffused X-rays as a function of the Doppler velocity v instead of the corresponding energy.

The observation of resonance is governed by the probability of emission (in the source) and absorption (in the absorber) of the gamma photons. This probability (Eq. (2)) is named the Lamb–Mössbauer or recoil-free factor. The probability of the interaction of a photon with a nucleus that is at the basis of the absorption is proportional to the square of the matrix element of the interaction Hamiltonian which excites the initial state i to the final state f:

$$f = \exp\left(-\frac{4\pi^2 E_\lambda^2 \langle x^2 \rangle}{(hc)^2}\right), \tag{2}$$

where x is the vibrational amplitude of the absorbing or emitting atoms in the solid lattice, E_γ the energy of the photon, and h is Planck's constant. The factor f can be expressed in the Debye model as follows:

$$f = \exp\left\{-\frac{3E_R}{2kT_D}\left[1 + 4\left(\frac{T}{T_D}\right)^2 \int_0^{T/T_D} \frac{y\,dy}{e^y - 1}\right]\right\}, \tag{3}$$

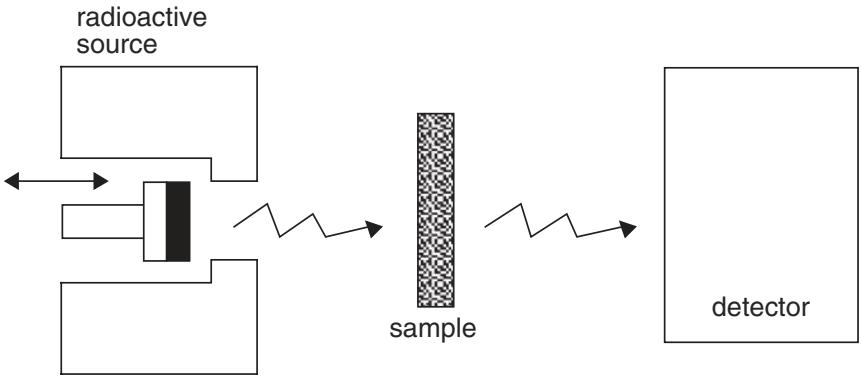

FIG. 1. Basic apparatus for measuring a Mössbauer spectrum in transmission mode.

where E_R is the recoil energy $\left(E_R = E_Y^2/2Mc^2\right)$, T the temperature, T_D the Debye temperature of the solid, and $y = hv/kT$. When $T \ll T_D$ and $T \ll T_D$, the expression may be approximated by

$$f_{T \ll T_D} = \exp\left\{-\frac{3E_R}{2kT_D}\left[1 + \frac{2\pi^2}{3}\left(\frac{T}{T_D}\right)^2\right]\right\} \quad \text{and} \quad f_{T \gg T_D} = \exp\left(-\left(\frac{6E_R}{kT_D}\frac{T}{T_D}\right)\right). \tag{4}$$

These equations are useful because they allow visualization of practical limits of the technique in terms of suitable isotopes, characteristics of the solids, and experimental conditions. Indeed, to have sufficiently large values of f, M should not be too small (≥ 40), E_γ not too large (≤ 150 keV), T_D not too small (which corresponds to relatively strong chemical bonds), and T not too high.

As a result of these constraints, 79 isotopes have been found for which the Mössbauer effect can be observed. For 38 of them, chemical perturbations of the nuclear levels result in resonance shifts or splittings of the order or greater than the observed width Γ_{exp} of the resonance line (this parameter is defined in the next paragraph (Eq. (9)) and can thus be used for Mössbauer spectroscopy. This list of 38 isotopes may be further restricted because of experimental difficulties encountered in their use. These difficulties are related either to their large recoil energies, which require a very low recording temperature for the spectra (4.2 K), or the short half-lives of the parent nucleides used as sources. In the former case, cryogenic cooling of both the source and the sample during the experiment may be needed; in the latter case, the manufacturing of the source requires rapid access to a nuclear reactor or accelerator.

In practice, by far the most commonly used Mössbauer isotopes in heterogeneous catalysis ($>90\%$ of all publications) are ^{57}Fe and ^{57}Co (in the emission mode). ^{119}Sn represents more than half of the remaining investigations, and most of the others have been done with a group of nuclei including ^{197}Au,^{193}Ir, ^{121}Sb, ^{125}Te, and ^{151}Eu.

In view of the importance of Ni, Ta, and Ru in catalysis, Mössbauer investigations of ^{61}Ni, ^{181}Ta, or ^{99}Ru would have been of great interest. Unfortunately, the aforementioned difficulties encountered with these isotopes lead to the realization that although Mössbauer spectroscopy is in principle possible, almost no investigations have been reported using these isotopes.

The magnitude of the observed absorption depends on the absorption cross-section for γ-rays to excite a transition between the nuclear ground and excited states at resonance. This cross-section per nucleus σ_0 is given by the following equation:

$$\sigma_0 = \frac{1}{2\pi}\frac{h^2c^2}{E_0^2}\frac{2I_e + 1}{2I_g + 1}\frac{1}{(1+\alpha)}, \tag{5}$$

where c is the velocity of light, E_0 the transition energy, I_e and I_g the excited and ground state spins, and α the internal conversion coefficient (α describes the relative probability of radiative (γ-ray) and non-radiative (electron conversion) processes of the transition (*2*)).

The magnitude of the observed resonance depends not only on σ_0 but also on the effective thickness of the absorber, which may be expressed as follows:

$$t = nf\sigma_0, \tag{6}$$

where n is the number of resonant isotope species per square centimeter. For small values of t (≤ 0.5) there is proportionality between the observed resonance intensity and t. For higher values of t, the proportionality no longer holds, and corrections have to be made to use the intensity values, for example, to establish the relative amounts of different phases.

Equation (5) gives the maximum value of the resonance absorption cross-section, which varies as follows with the energy:

$$\sigma = \sigma_0 \left[1 + \frac{4(E - E_0)^2}{\Gamma_0^2} \right]^{-1}, \tag{7}$$

where E is the incident energy and Γ_0 the width of the excited nuclear state. This width is given by Heisenberg's uncertainty relationship:

$$\Gamma_0 = \frac{h}{2\pi\tau}, \tag{8}$$

where τ is the mean (or natural) exponential lifetime of the excited state ($1.44 \times$ the half-lifetime). Because the source radiation and the absorber cross-section have line width values of Γ_0, the minimum width actually observable in a transmission experiment is $2\Gamma_0$. This corresponds approximately to 0.2 mm/s of velocity Doppler shift for ^{57}Fe (and 0.65 mm/s for ^{119}Sn). The broadening of the line width beyond this theoretical value is related to inhomogeneities arising from imperfections in the source or the absorber or from a saturation effect. The observed experimental line width is evaluated, and an approximate value can be calculated from the following equation:

$$\Gamma_{\text{exp}} = \Gamma_0(2 + 0.27t_{\text{A}}), \tag{9}$$

where t_{A}, called sample or absorber thickness, equals $f_{\text{A}} n_{\text{A}} a \sigma_0 t$, with f_{A} being the Lamb–Mössbauer factor of the absorber, n_{A} the number of resonant isotope species per cubic centimeter, and a the fractional abundance of the Mössbauer isotope. Generally, t_{A} has to be optimized experimentally, and values close to or smaller than 1 are used. Because the cross-section has a Lorentzian shape $1/(1 + x^2)$ form around E_0 (Eq. (7)), the resonance peak has the same shape.

B. Hyperfine Interactions and Mössbauer Parameters

The nuclear ground and excited levels involved in the Mössbauer transition are shifted or split because of the electrostatic interactions between the nuclear charge and the surrounding electric charge (Fig. 2). The first interaction, sometimes called the electric monopole interaction, shifts only the nuclear levels and is related to the perturbation resulting from the electrons inside the nuclear volume. This shift is

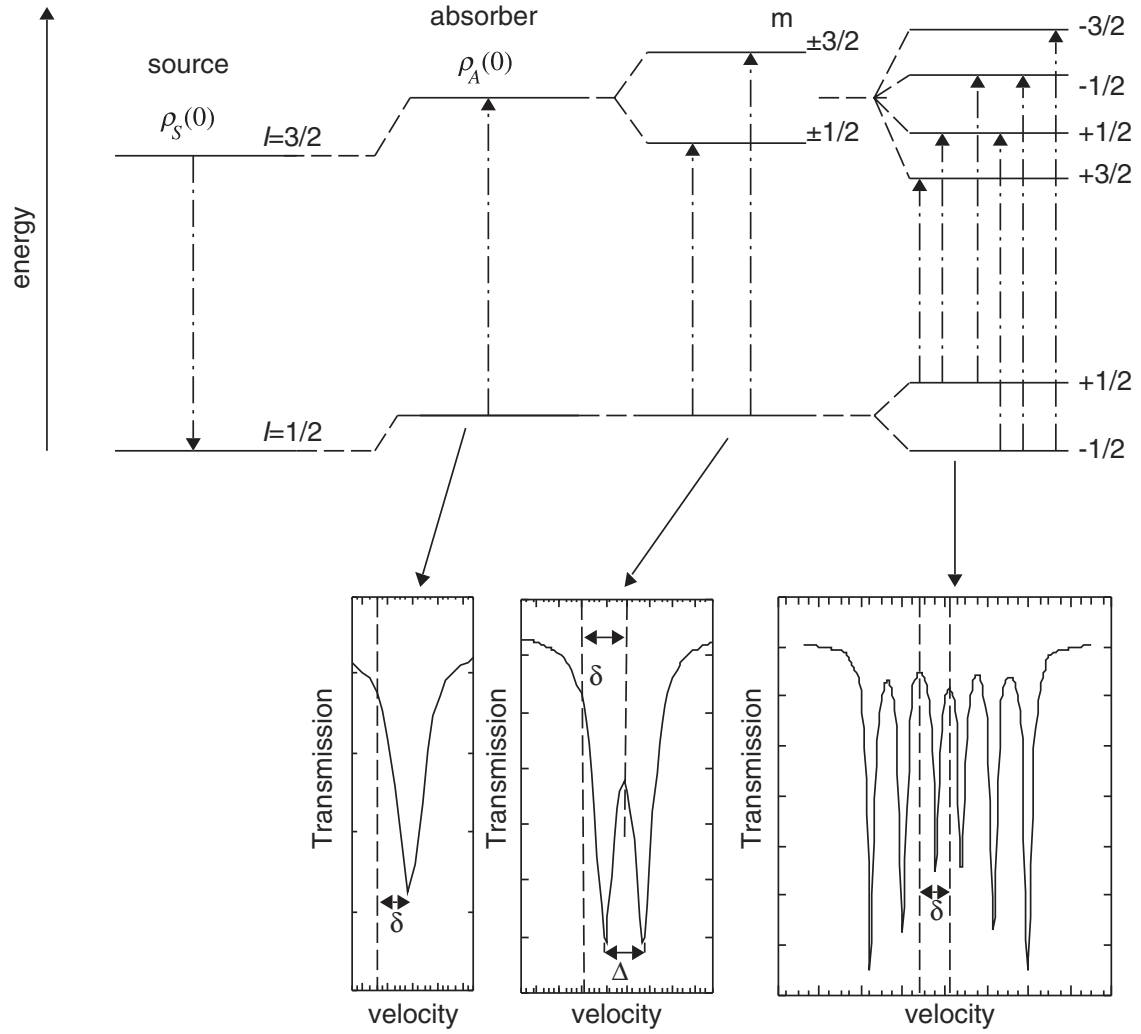

FIG. 2. Schematic representation of the hyperfine interactions in the case of a Δ transition $1/2 \rightarrow 3/2$ like that of ^{57}Fe.

different for the ground and excited states because the nuclear volumes are different in the two states. Furthermore, these shifts are different for the source and the absorber because emitting and absorbing nuclei have different electron densities inside the nuclear volumes because of different chemical states and electronic environments, and the absorption will be observed at a velocity characteristic of the absorber relative to the source. This measured shift, called isomer shift (*IS*), is expressed as follows:

$$IS = \frac{2}{3} e^2 \pi Z S(Z) \Delta \langle r^2 \rangle \left[\rho_{\mathrm{A}}(0) - \rho_{\mathrm{S}}(0) \right], \tag{10}$$

where $\Delta\langle r^2 \rangle$ is the variation of the mean-square radius of the nucleus between the excited and ground states of the Mössbauer transition, $S'(Z)$ is a correction for the relativistic effects, and the term in brackets, $\rho_{\mathrm{A}}(0) - \rho_{\mathrm{S}}(0)$, the difference between the electron density at the nucleus in the absorber A and the source S.

Isomer shifts measured and defined as in Eq. (10) depend on the source. For a comparison of results reported by different authors, these must be stated with respect to that of a standard compound. In the case of ^{119}Sn, the usual standards

are $BaSnO_3$ and SnO_2, and in the case of ^{57}Fe, they are α-Fe metal or sodium nitroprusside. The latter compound is, however, used less and less. For Mössbauer nucleides other than these two, there are generally no specific prescriptions regarding standards. In some cases, the natural line width is very broad relative to those of iron or tin, or the change in nuclear radius between the ground and the excited state is very small so that the measurement of isomer shifts is difficult or virtually impossible. The use of an isomer shift standard thus became insignificant.

Although IS is independent of T, variations with temperature are observed experimentally because IS_{OBS} is in fact a linear combination of IS and a second shift which is sample-dependent, being called a second-order Doppler shift (SOD):

$$IS_{OBS} = IS + IS_{SOD}. \tag{11}$$

This shift arises from the relative motions associated with atomic vibrations, via a second-order relativistic effect; it is equal to the following:

$$IS_{SOD} = -\frac{\langle V^2 \rangle}{2c^2} E_y, \tag{12}$$

where $\langle V^2 \rangle$ is the mean-square velocity of the probe nucleus in the sample, which can be derived from the Debye model of the vibrations:

$$IS_{SOD} = -\frac{1}{2c}\frac{9kT_D}{8M}\left[1 + 8\left(\frac{T}{T_D}\right)^4 \int_0^{\frac{T}{T_D}} \frac{y^3 \mathrm{d}y}{e^y - 1}\right]. \tag{13}$$

It is evident that this term depends on the temperature and also on the source and the absorber (through M and T_D).

A second perturbation of the nuclear levels is caused by the magnetic interaction between the nuclear magnetic moment and the surrounding electron spin density, creating an electric field gradient at the nucleus. This electric field gradient is a tensor that is described by the spatial orientations of its three principal axes U_{XX}, U_{YY}, and U_{ZZ}.

This interaction partially removes the degeneracies of nuclear states in which the nuclei have non-zero quadrupole moments Q (spin $I > 1$) into $2I + 1$ nuclear states characterized by the value of the magnetic quantum number m_I, and it shifts them. In the general case when the electrical field gradient has no axial symmetry, the energy shift of the levels can be expressed as follows:

$$E_Q = eU_{ZZ}Q\frac{3m_I^2 - I(I+1)}{4I(2I-1)}\left(1 + \frac{\eta^2}{3}\right)^{1/2}, \tag{14}$$

where Q is the quadrupole moment of the nucleus in the excited state of the Mössbauer transition, m_I the magnetic quantum number, U_{ZZ} the main component of the electric field gradient tensor ($|U_{ZZ}| > |U_{YY}| \geq |U_{XX}|$), and η the asymmetry parameter ($\eta = (U_{XX} - U_{YY})/U_{ZZ}$), which is zero in the case of axial symmetry.

In the case of ^{57}Fe, the ground state is an $I = 1/2$ state without a quadrupole moment and is thus not affected by the electric field gradient. The first excited state is an $I = 3/2$ state with a quadrupole moment and has a degeneracy of 4 that is

partially lifted. It is symmetrically split into two substrates. This splitting, called quadrupolar splitting (QS or Δ), is given by the following:

$$\Delta = \frac{1}{2} e U_{ZZ} Q \left(1 + \frac{\eta^2}{3}\right)^{1/2}. \tag{15}$$

As a result, the Mössbauer spectrum will consist of two lines, called a doublet, with a $2\Gamma_0$-line width and separated by Δ, the isomer shift being measured at the center of the doublet (Fig. 2). The relative intensities of the two absorption lines of the doublet depend on the orientation of U_{zz} relative to the incident X-ray direction (Table I). For a fine powder absorber, in which all directions are uniformly distributed, the two lines of the corresponding doublet have equal intensities.

A third perturbation of the nuclear energy levels occurs in the presence of a magnetic field and yields different energies for the different orientations of the nuclear magnetic moment m_I relative to the field direction. Each nuclear level of non-zero spin is shifted into $2I+1$ sub-levels reached by shifting it by $-g\mu_N m_I H$, where H is the magnitude of the magnetic field, g the nuclear factor of the considered sub-level, and μ_N the nuclear Bohr magneton.

For example, in the case of iron, the ground level will undergo a symmetric splitting ($I = 1/2$, $m_I = +1/2$, $m_I = -1/2$) and the first excited state is split into four sub-levels ($I = 3/2$, $m_I = +3/2$, $m_I = +1/2$, $m_I = -1/2$, $m_I = -3/2$). Among the eight possible transitions between the two sub-levels of the ground state and the four sub-levels of the excited state only six are allowed by the quantum mechanical selection rule, and the resonance spectra consist of six lines with a $2\Gamma_0$-line width called a sextet. The isomer shift is measured at the center of the sextet (Fig. 2). H is proportional to the difference between the positions of two lines of the spectrum; the outermost ones are generally considered in the data analysis for better precision.

TABLE I

Line Position and Relative Intensities in ^{57}Fe Spectra Obtained in the Presence of an Electric Field Gradient (Doublet) and both an Electric Field Gradient and a Magnetic Field (Sextet)

	Line	Spin state		Line position (mm/s)	Relative intensities
		I_g	I_e		
Doublet	1	$\pm 1/2$	$\pm 1/2$	$\delta - \Delta/2$	$2 + 3\sin^2\theta_{\gamma VZZ}$
	2	$\pm 1/2$	$\pm 3/2$	$\delta + \Delta/2$	$3(1 + \cos^2\theta_{\gamma VZZ})$
Sextet	1	$+1/2$	$-3/2$	$\delta - (Z+3)(z/2) + \varepsilon$	$3(1 + \cos^2\theta_{\gamma H})$
	2	$+1/2$	$-1/2$	$\delta - (Z+1)(z/2) - \varepsilon$	$2(2\sin^2\theta_{\gamma H})$
	3	$+1/2$	$+1/2$	$\delta - (Z-1)(z/2) - \varepsilon$	$1(1 + \cos^2\theta_{\gamma H})$
	4	$-1/2$	$-1/2$	$\delta - (Z-1)(z/2) - \varepsilon$	$1(1 + \cos^2\theta_{\gamma H})$
	5	$-1/2$	$+1/2$	$\delta - (Z+1)(z/2) - \varepsilon$	$2(2\sin^2\theta_{\gamma H})$
	6	$-1/2$	$+3/2$	$\delta + (Z+3)(z/2) + \varepsilon$	$3(1 + \cos^2\theta_{\gamma H})$

$\theta_{\gamma VZZ}$ and $\theta_{\gamma H}$ are respectively the angles between the gamma ray direction, V_{zz} and H. I_g and I_e are the spin states of the ground and excited states; Δ the quadrupolar splitting (Eq. (15)), and ε the quadrupolar shift parameter (Eq. (16)). Z the ratio between the g factor of the ground (g_i) and excited state (g_e), and $z = g_e \mu_N H$.

In the presence of a small simultaneous electric quadrupolar interaction, the split levels are shifted by an amount ε, which is called the quadrupole shift parameter and is given by the following:

$$\varepsilon = \left(\frac{e^2 U_{zz} Q}{8}\right)[2 - (3 - \eta \cos 2\phi)\sin^2\theta], \tag{16}$$

where ϕ and θ are the azimuthal and polar angles of the magnetic field direction in the principal axes coordinate system of the electric field gradient. The relative intensities of the six lines of the sextet depend on the orientation of the magnetic field relative to the incident γ-ray beam (Table I).

The magnetic field can have several origins and may be written as the sum of up to five contributions that can be added vectorially to give the following expression:

$$H = H_{\mathrm{S}} + H_{\mathrm{L}} + H_{\mathrm{D}} + H_{\mathrm{M}} + H_{\mathrm{E}}, \tag{17}$$

where H_S, H_{L}, and H_{D} are, respectively, the fields attributed to the s-electron spin polarization term, to the on-site orbital electron current, and to the dipole interaction related to the local electron spin moments on the probe site. H_M is the field resulting from the magnetization of the particle within which the nucleus is located. It depends on the shape and magnetic domain structure of the particles. H_{E} is an external magnetic field that can be applied to the sample.

C. Spectral Analysis and Interpretations

In the preceding section the hyperfine parameters (δ, Δ, H, and f) that can be extracted by spectral analysis were presented. These parameters have complex relationships with physico-chemical properties that are presented in a rather simplified manner in the following section, showing how local electronic, magnetic, structural, and chemical environments can be characterized.

Equation (10) shows that the isomer shift *IS* is a direct measure of the total electronic density at the probe nucleus. This density derives almost exclusively from *s*-type orbitals, which have non-zero electron densities at the nucleus. Band electrons, which have non-zero occurrence probabilities at the nucleus and *s*-type conduction electrons in metals may also contribute, but to a lesser extent. Figure 3 shows the linear correlation that is observed between the experimental values of ^{121}Sb Mössbauer isomer shift and the calculated values of the valence electron density at the nucleus $\rho_v(0)$. The total electron density at the nucleus $\rho_{\mathrm{A}}(0)$ (Eq. 10) is the sum of the valence electron density $\rho_v(0)$ and the core electron density $\rho_c(0)$, which is assumed to be constant. This density is not only determined by the *s*-electrons themselves but also by the screening by other outer electrons (*p*-, *d*-, or *f*-electrons) and consequently by the ionicity or covalency and length of the chemical bonds. *IS* is thus a probe of the formal oxidation state of the isotope under investigation and of the crystal field around it (high- and low-spin Fe^{2+} may be differentiated). The variation of *IS* with temperature can be used to determine the Debye temperature of a compound (see Eq. (13)).

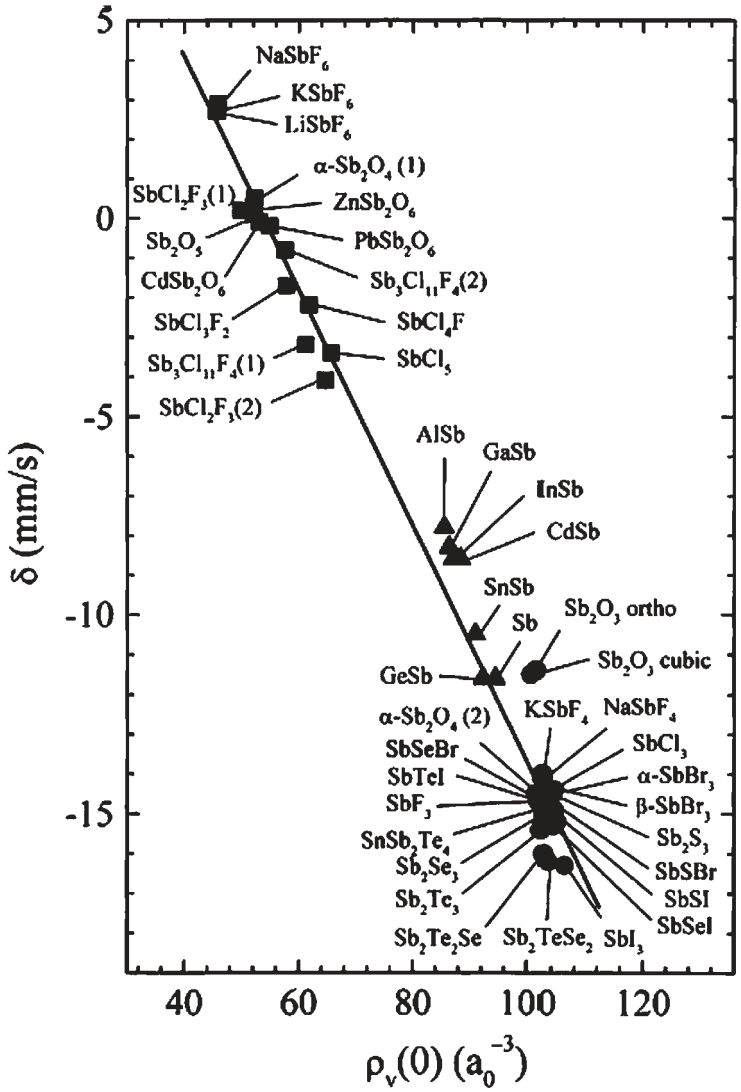

FIG. 3. Linear correlation between the experimental values of the ^{121}Sb Mössbauer isomer shift δ (relative to $BaSnO_3$) and the calculated values of the valence electron density $\rho_v(0)$ at the nucleus for a series of compounds. $\rho_s S(0) = \rho_v(0) + \rho_c(0)$, where $\rho_c(0)$ is the core electron density, which is assumed constant. Figure according to Lippens (*7*).

The quadrupolar splittings depend mainly on the electric field gradient at the nucleus, which is caused by the spatial distribution of the electrons around it, via electric Coulomb forces. Both electrons (valence contribution U_{val}) and neighboring anions and cations (lattice contribution U_{lat}) in the vicinity of the nucleus contribute to this electric field gradient U, which can be expressed as follows:

$$U = U_{\text{val}}(1 - R) + U_{\text{lat}}(1 - \gamma), \tag{18}$$

where R and γ are screening and anti-screening Sternheimer parameters. Values of R range between 0 and 1, and values of γ between -10 and -100. Because of these two contributions, the quadrupolar splitting is strongly related to site symmetry and local structure. For example, in the case of iron, if the site being characterized is a $Fe^{3+}(4s^x 3d^5)$ ion, inner atomic shells are spherically symmetric, and q_{val} is the

major component of the electric field gradient). In contrast, $Fe^{2+}(4s^x3d^6)$ ions have asymmetric distributions of their valence electrons, and q_{val} has a dominant contribution to the electric field gradient. The quadrupolar splitting characterizes the degree of local asymmetry at the probe site. Such local asymmetry is caused by various forms of structural, chemical, and magnetic disorder, such as lattice defects, chemical substitutions of neighboring anions, local moment disorder in magneto-volume and magneto-elastic materials that can be characterized and quantified in solid catalysts.

For example, the Mössbauer spectrum of a $BaFe_3Al_9O_{19}$ catalyst for combustion of methane is given in Fig. 4 (*8*). This spectrum has been fitted with four sextets that correspond to the four octahedral crystallographic sites of the structure that may be occupied by the ferric ions, thus leading to a different atomic environment for each of them. From the relative intensities of the four sextets used for the fit and considering equal *f* factors for the corresponding species, it is possible to determine the respective occupation of these sites by iron. Alternatively, only a complete Rietveld analysis of the powder X-ray diffraction pattern of the catalyst would have enabled such a determination.

The internal magnetic field *H* is a reliable signature of a given species and allows a good identification of magnetic phases containing these species. In catalyst characterization, one of the major interests in this last parameter relates to its variation with temperature, which can be used to evaluate particles sizes and particle size distributions when the particles are small enough. Indeed, when particles of a magnetic phase are small, a collective reorientation of the magnetic moment is observed in these particles. In a large particle, once a particular orientation has been reached below the magnetic ordering temperature, it does not change, and an internal magnetic field is observed leading to a sextet in the Mössbauer spectrum. When particles are small, the thermal excitation energy can be sufficiently high to invert all of the spins simultaneously, thereby reversing the magnetization of the lattice. If the relaxation time (τ_r) of these inversions is smaller than the nuclear Larmor precession time (τ_L), the magnitude of the magnetic field at the nucleus averages to zero, and no magnetic splitting is observed. The solid behaves as a paramagnetic solid (superparamagnetic behavior), which results in the observation of a doublet instead of a sextet in the Mössbauer spectrum.

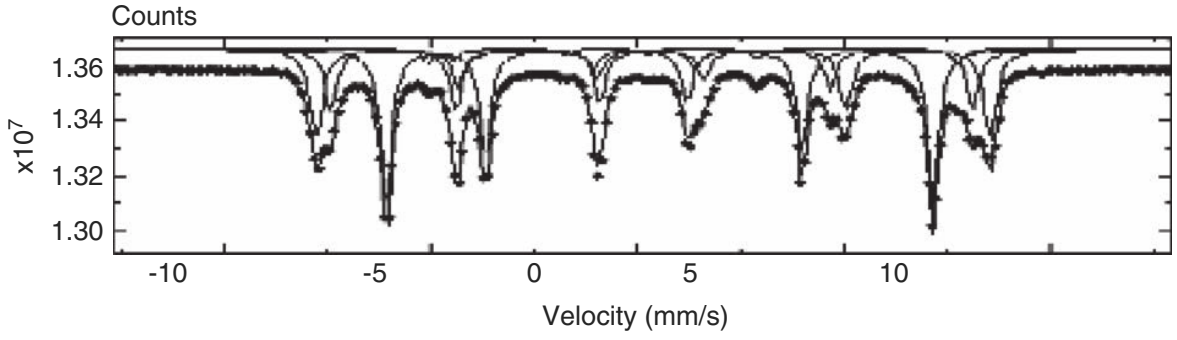

FIG. 4. Mössbauer spectrum of a $BaFe_3Al_9O_{19}$ catalyst recorded at 298 K in air. Solid lines are derived from least-square fits. Figure according to Naoufal *et al.* (*8*).

The relaxation time can be expressed in a simplified manner as follows:

$$\tau_r = \tau_0 e^{KV/kT}, \tag{19}$$

where K is the anisotropy constant and V the volume of the particle. It is clear that τ_r increases with decreasing temperature and can become larger than τ_L. In such cases, the spectrum changes, and a sextet is again observed.

A simplified method was proposed by Kündig *et al.* (*9*) allowing evaluation of the particle size and the size distribution of a solid by analysis of its spectrum as a function of temperature. By variation of the temperature it is possible to follow the variation of the relative spectral areas of the sextet and doublet. Assuming that particles for which $\tau_r < \tau_L$ and $\tau_r > \tau_L$ contribute exclusively to one of the two components (paramagnetic and magnetic), the temperature at which $\tau_r = \tau_L$ and at which the hyperfine split takes place can be determined; V is calculated from Eq. (19) at the temperature T at which the spectral areas of the two components are equal). The dependence of the two spectral areas on temperature in the range in which both components are observed yields the particle size distribution.

One can often describe a solid catalyst as a dispersed set of active species on the surface of a support, present as more or less isolated atoms or small particles. These species, because of their small size and their bonding to the support, present specific features different from those of bulk material. Many studies of supported catalysts have shown that the f factor for small particles is influenced by the vibration of the particles relative to the atomic environment. It may therefore be difficult to unravel contributions of surface vibrations to the f factors of small particles. On the other hand, when active species are weakly adsorbed at the surface of a support, they can also vibrate or even diffuse on the surface, leading to a decrease of their f factors and to a broadening of the lines in the Mössbauer spectra that can result in the disappearance of the signal. Furthermore, if they only vibrate, the mean-square vibration amplitude perpendicular to the surface is not the same as that parallel to the surface, leading to an anisotropy of the f factor. This effect (referred to as Karyagin–Goldanskii effect) implies a dependence of f upon θ (the angle between U_{zz} and the direction of the incident γ-radiation). In the case of a doublet, an asymmetry of the intensity of the two lines is observed; this may complicate spectral analysis.

Another difficulty may arise from the deviation from a Lorenzian line shape of the absorption signal. Such deviation corresponds to either homogeneous or inhomogeneous broadening. Inhomogeneous broadening relative to the natural line width is caused by variable environments of the probe nuclei that create variations in the electronic or structural characteristics. This broadening can be considered to be a consequence of the superposition of many sub-spectra and can relatively easily be taken into account by fitting the experimental spectra considering a distribution of sub-spectra with Lorenzian line shapes. Homogeneous broadening originates from time variation in the electronic environment. Such effects, referred to as relaxation effects, imply the modification of the line width of the elemental spectrum. These broadenings may coexist and significantly complicate the analysis and interpretation of Mössbauer spectra.

D. Related Techniques

D.1. *Emission Mössbauer Spectroscopy (EMS)*

In Mössbauer absorption spectroscopy, as described in the preceding section, an emitting moving source with a single-line resonance is used to scan the energy levels of an absorber that is the material under investigation. In contrast, in Mössbauer emission spectroscopy, the source corresponds to the material under investigation and a reference single-line absorber has to be used. The studied emitting material can be moved but most of the times it is the reference absorber that is moved (Fig. 5). This technique has been used successfully to investigate $CoMo/Al_2O_3$ catalysts, which are well known for their use in hydrotreating processes. The technique has contributed to identify the active species of these catalysts (*10,11*).

The catalysts to be investigated with this method should be synthesized with radioactive ^{57}Co; this constitutes the major experimental challenge of the technique. Another challenge may be encountered in the interpretation of the MES spectra. This interpretation may be hampered by the so-called chemical aftereffects. The transition from ^{57}Co to ^{57}Fe occurs in the catalyst via electron capture, whereby the electronic structure of the atom is changed. This change is followed by a reshuffling of the electrons in the material that may take time to occur, especially if the material is an insulator. If this required time is longer than the lifetime of the excited state, the probed electronic structure and, thus, the energy levels may have changed. Therefore, EMS is generally applied as a fingerprint technique, with spectra being compared to each other and to those of reference compounds.

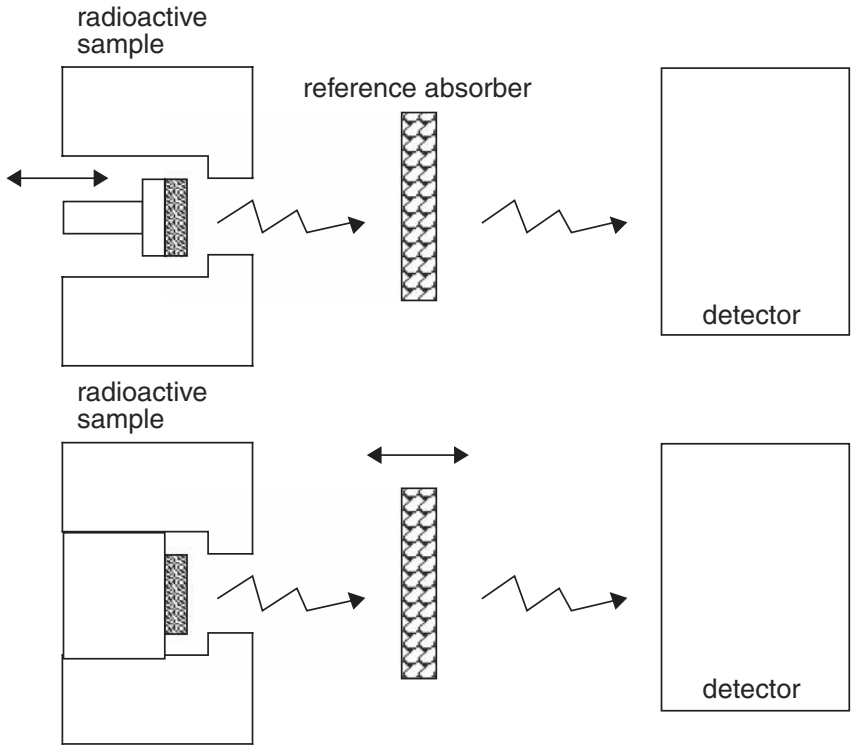

Fig. 5. Basic equipment for measuring an emission Mössbauer spectrum. The sample is prepared with a radioactive isotope and used as the source.

The single-line absorber is generally potassium (or sodium) nitroprusside, $K_4Fe(CN)_6,3H_2O$, enriched with ^{57}Fe.

Besides hydrotreating catalysts (*12–20*), supported cobalt Fischer–Tropsch catalysts (*21–25*) and multi-phasic molybdate-containing catalysts for propene oxidation (*26*) have also been characterized by this technique. The technique can also be applied for investigations involving ^{107}Cd, ^{133}Cs, ^{195}Pt, ^{99}Rh, and ^{83}Rb.

D.2. *Conversion Electron Mössbauer Spectroscopy (CEMS)*

It is possible to analyze the fluorescence radiation emitted from the decay of the excited state in the solid instead of the absorption of the gamma X-rays. This can be done by detecting and analyzing the conversion electrons arising from the internal conversion process in which the de-excitation leads to the ejection of an inner-shell electron instead of being used in the production of a γ-radiation (Fig. 6). This internal conversion process is much more frequent than X-ray emission. The initial kinetic energy of an ejected conversion electron is equal to the energy of the transition minus its original atomic binding energy. Because emitted electrons lose energy as they interact with the sample, their path length is limited to 0.1–0.2 μm, and therefore CEMS is a surface-sensitive technique. It is possible to analyze the energy distribution of the ejected electrons and to obtain spectra with various depth resolutions (depth-selective CEMS is called DCEMS). Ultrahigh-vacuum and high-resolution spectrometers allow analysis of surface layers with thicknesses as low as 1 nm with almost atomic-scale depth resolution.

This technique is used only infrequently in catalysis research. For finely dispersed catalysts, the size of the particles is smaller than the depth analyzed, and spectra are

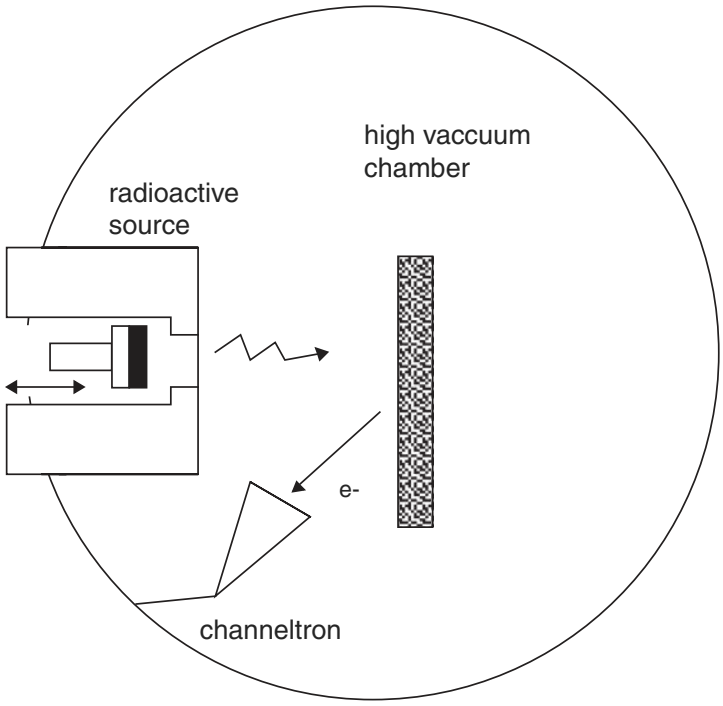

FIG. 6. Basic equipment for measuring a conversion electron Mössbauer spectrum.

consequently similar to those recorded in the conventional transmission mode. Furthermore, the high-resolution analysis of a fine-powder sample is sometimes difficult to achieve, and the use of ultrahigh vacuum may lead to surface modification of the sample. Therefore, CEMS has found limited applications in the field of catalysis.

This technique has been reviewed recently, and applications to surface characterization were described in Reference (*27*).

It is noteworthy that a low-temperature apparatus has been described recently that allows γ-ray and conversion electron Mössbauer spectroscopy measurements at the same time, in the temperature range from 10 K to room temperature (*28*).

III. Applications of Mössbauer Spectroscopy in Heterogeneous Catalysis

In this section, we summarize results characterizing catalytic materials by Mössbauer spectroscopy. An analysis of the literature leads to the following classifications of the objectives of this work:

1. Identification of catalyst components in terms of active phase or active sites and search for correlations between these components and one or more of the catalytic properties.
2. Investigations of catalysts under working conditions and analysis of activation or deactivation processes that may take place with time on stream.
3. Study of chemisorption of reactants or molecular probes.

Progresses and recent results obtained in each category are presented below. Our intent is to give a broad view of the results generated recently, and this review is not exhaustive.

A. Identification of Catalyst Components

Mössbauer spectroscopy has been quite successful in identifying catalyst components. Mössbauer spectroscopy provides quantitative site populations, easily discriminating between various metal oxidation states and anion coordinations, and it can lead to phase compositions or distributions between phases of the isotope under investigation. It also gives quantitative population distributions of local distortion environments and local chemical environments, via extracted quadrupolar splitting distributions.

The majority of investigations in this category has dealt with the isotopes ^{57}Fe, ^{119}Sn, and ^{57}Co (in emission mode). In contrast, investigations focusing on other isotopes, such as ^{197}Au, ^{121}Sb, ^{125}Te, ^{193}Ir, or ^{99}Ru, have been limited in number but very fruitful.

A.1. *Iron-Containing Catalysts*

^{57}Fe Mössbauer spectroscopy has been used extensively to characterize catalysts, constituting the large majority of the Mössbauer investigations of catalysts. The

publications dealing with the Mössbauer spectroscopy of iron-containing catalysts cover a broad range, and only a partial coverage of the work is included here. These investigations focus mainly on well-known reactions for which iron-containing catalysts are among the best. These reactions are the Fischer–Tropsch synthesis (*29–50*), ethylbenzene dehydrogenation (*51–58*), ammonia synthesis (*59–71*), the water gas shift (*72–75*), and oxidation reactions (*76–90*). In addition to these catalysts for these reactions, several others have been the focus of Mössbauer investigations, including those concerned with catalytic materials that have attracted recent attention, such as iron supported on ZrO_2 (*91–104*) or MgO, either directly prepared from MgO (*105–107*) or from substituted hydrotalcite (*108–111*). Zeolites and mesoporous materials (*112–125*), especially ZSM-5 (*120–125*) and MCM-41 (*112–128*) were also investigated. Furthermore, bimetallic alloys have also been characterized by Mössbauer spectroscopy (*129–149*) to determine the active phases and active sites.

A.2. *Tin-Containing Catalysts*

The characterization of tin-containing catalysts by Mössbauer spectroscopy has been focused mainly on supported bimetallic alloys (*150–162*). These catalysts, which consist of Pt, Pd, Rh, or Ru as primary metals with Sn used as a promoter, are generally supported on SiO_2 or Al_2O_3. These catalysts are used in reforming and hydrogenation processes in the petroleum industry (*151,152*) and have recently drawn attention for other applications, such as low-temperature CO oxidation, alkane and alcohol dehydrogenation, metathesis reactions (*153–160*), and even nitrate removal for drinking water processing (*161*).

The Mössbauer transition in the isotope ^{119}Sn is of the same type as that occurring in ^{57}Fe ($1/2 \rightarrow 3/2$). Depending upon the presence or absence of an electric field gradient at the nucleus, single lines or doublets are observed. Mössbauer spectroscopy appears to be efficient for identification and quantifications of various compounds that are formed, depending upon the nature of the support, the metal relative contents and the preparation conditions; these include Pt_3Sn, PtSn, $PtSn_2$, or SnO and SnO_2. Preparation of these catalysts by the contacting of silica-supported rhodium with tetra-*n*-butyl-tin, led to relatively stable solids with organometallic fragments bonded to the rhodium surface. These materials may exhibit very high selectivities and activities for hydrogenation of α,β unsaturated aldehydes or nitrobenzene (*159*). Mössbauer spectroscopy has allowed identification of all the species that were encountered when tetra-*n*-butyl-tin interacted with the surfaces of silica or silica-supported rhodium (Fig. 7). At room temperature, tetra-*n*-butyl-tin was physically adsorbed on the surfaces (characterized by a single line $\delta = 1.42$ mm/s). After reaction under H_2 at 373 K, the formation of grafted organometallic fragments on the rhodium surface (characterized by a doublet with $\delta = 1.39$ and $\Delta = 2.26$ mm/s) as well as a well-defined bimetallic RhSn compound (characterized by a doublet $\delta = 1.42$ and $\Delta = 0.85$ mm/s) were identified, whereas with pure silica, surface-bound $\equiv$Si–O–Sn(n-C_4H_9)$_3$ moieties were observed (characterized by a doublet $\delta = 1.39$ and $\Delta = 2.69$ mm/s). After treatment at 523 K, the rhodium-grafted organometallic species were completely decomposed,

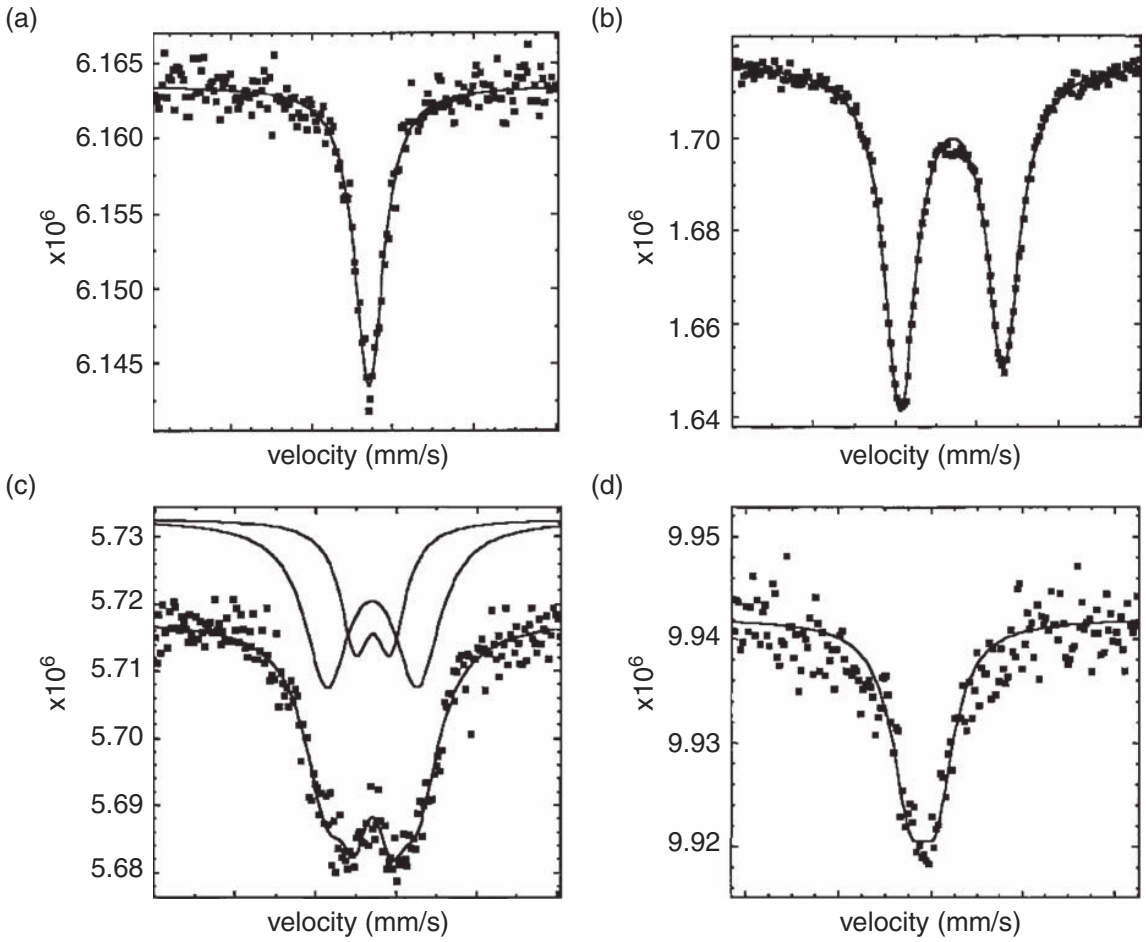

FIG. 7. Experimental Mössbauer spectra of samples recorded at 78 K: (a) $Sn(n\text{-}C_4H_9)_4$ physisorbed on SiO_2, (b) $\equiv SiOSn\text{-}(n\text{-}C_4H_9)_3$, (c) $Rh_s[Sn(n\text{-}C_4H_9)_2]/SiO_2$, and (d) $Rh_s[Sn(n\text{-}C_4H_9)_2]/SiO_2$ treated at 523 K. Solid lines are derived from least-square fits. Figure according to Millet *et al.* (*158*).

and formation of a well-defined bimetallic RhSn compound was observed. Because the isomer shift of Pt–Sn alloys of varying composition varies linearly with the Sn mole fraction (*160*), it was possible to determine the composition of the alloy-like structures and consequently the relative amount of the grafted species. This quantification was confirmed by use of X-ray photoelectron spectroscopy.

Mesoporous tin-containing analogues of MCM-41 and tin oxide-modified mesoporous SBA-15 have also been characterized by Mössbauer spectroscopy (*162,163*). In the first case, the results suggest that tin was incorporated in the structure of the silicate and, in the second, they indicated that two types of supported tin species were formed, depending on the tin content. One would correspond to atomically isolated species stabilized in the wall of the pore and susceptible to reduction to Sn^{2+} under reductive treatment conditions and the other to large oxide clusters distributed in the external pore structure.

A.3. *Gold-Containing Catalysts*

Highly dispersed supported gold has been shown to have high catalytic activity for various oxidation reactions ^{197}Au spectroscopy has emerged as one of the

methods of choice for investigation of catalysts consisting of gold particles on oxide supports, such as TiO_2, Fe_2O_3, SiO_2, Al_2O_3, MgO, and MnO_x (*164–170*). The ^{197}Au resonance is characterized by I_g and I_e, respectively, equal to 3/2 and 1/2. Consequently, the presence of an electric field gradient at the nucleus does not affect the excited state, although the ground state is symmetrically split into two sub-states. This splitting leads to the presence of doublets in the spectra.

Early investigators proposed the presence of both metallic and ionic gold species (Au^{III}) in the active catalysts (*165*), but more recent investigations suggest the presence of only metallic species (*166,167*). Mössbauer spectra obtained for gold catalysts supported on TiO_2 and SiO_2 are shown in Fig. 8. The solid lines in the figure are derived from least-squares fits and show both the total fits and the sub-spectra. The spectra are fitted using a single line ($IS = -1.22$ mm/s), which is attributed to bulk gold, and a doublet that has been attributed to surface metallic species ($-1.5\,\text{mm/s} < IS < -0.75\,\text{mm/s}$ and $1.25\,\text{mm/s} < QS < 2.5\,\text{mm/s}$). Indeed, since the earlier Mössbauer investigations of gold compounds (*168,169*), it was observed that isomer shifts (*IS*) and quadrupolar splittings (*QS*) vary over a wide range.

This variation could have rendered difficult the attribution of oxidation states to the detected species, but it was shown that a linear correlation between *IS* and *QS* values exists for Au^{I} and Au^{III} compounds (*170*). This relationship has been

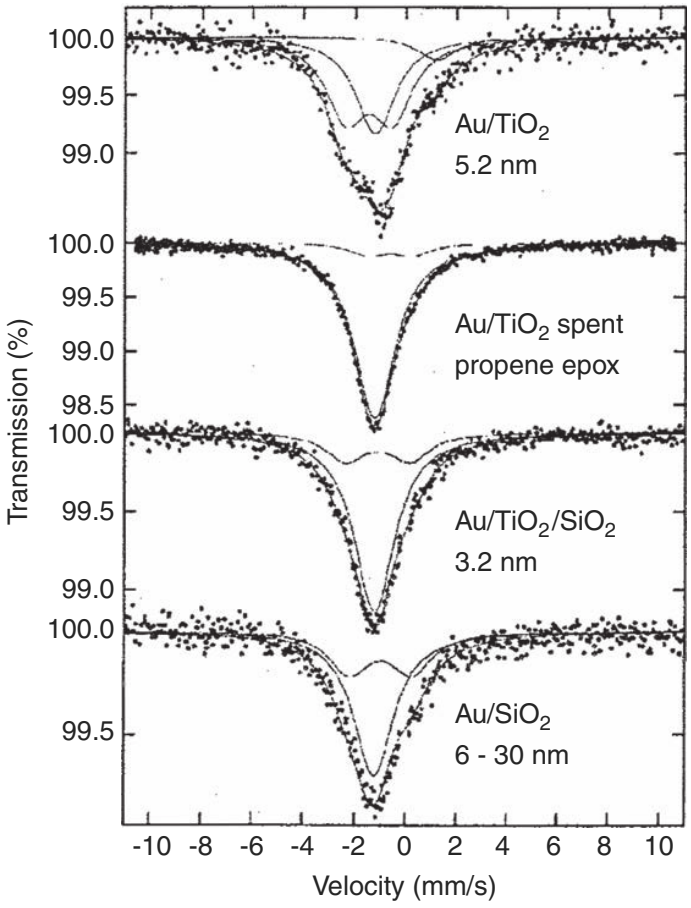

FIG. 8. Mössbauer spectra recorded at $T = 4.2$ K of gold catalysts on various supports used for propene epoxidation. The average size of the particles is given in the legend. Figure according to Goossens *et al.* (*165*).

explained by the fact that for a given oxidation state the effective charge on the gold atom does not vary as a result of π-back donation, and only transfers between the *d*- and *s*-shells are observed, which affect both *IS* and *QS* values. This is possible because the lattice contribution to *QS* is at least one order of magnitude smaller than the contribution of the valence electrons (Eq. (18)). To determine whether the observed doublet could be attributed to ionic species, the *IS*/*QS* combinations have thus been considered, and it has been observed that they did not fit within ranges corresponding to Au^{I} and Au^{III}. Moreover, the isomer shifts always remained close to that of the bulk species. It was thus proposed that they correspond to metallic surface species, the presence of a *QS* being only related to the large electric field gradient generated at the surface of the gold particles (*166*). The Au/TiO_2 spectrum (upper plot of Fig. 8) still showed a small contribution that might be attributed to Au^{V} that has not been explained but which disappeared after catalysis and was never observed on any other support. A recent study on Au/Fe_2O_3 confirmed the exclusive presence of metallic gold Au^{0} on the catalysts but only after heat treatment at high temperature (400° C) (*170*). At lower temperature, at which the catalysts were more active, both Au^{III} (probably related to the presence of $AuOOH,H_2O$) and Au^{0} were observed. Although discrepancies remain in the literature on the existence and role of the gold species, Au^{0} and/or Au^{III} were most of the time identified by Mössbauer spectroscopy in the catalysts and may both play a role; conversely Au^{I} was never observed in the catalysts suggesting that its involvement is very unlikely.

A.4. *Antimony-Containing Catalysts*

^{121}Sb Mössbauer spectroscopy has been used to investigate the tin-antimony oxide catalysts used for selective oxidation of hydrocarbons (*171*). Recent investigations have been conducted to characterize FeSbO catalysts for ammoxidation of propene (*172*) and VSbO (*173*) and MoVSbNbO (*174*) catalysts for ammoxidation of propane.

The Mössbauer transition for the ^{121}Sb isotope is of the type $5/2 \rightarrow 7/2$. Broad, asymmetric lines indicating unresolved quadrupolar split spectra are observed for the oxide compounds (Fig. 9). However, the relative variation of the nuclear radius $\left(\Delta\langle r^2\rangle\right)$ is rather large, and therefore the isomer shift for this system becomes a sensitive parameter not only for changes in oxidation state but also for changes in the local environment. Isomer shifts allow the identification and characterization of various ionic species. In the cases of VSbO and FeSbO, the investigations evidenced the presence of β-Sb_2O_4 formed during the synthesis or by segregation under catalytic condition. In the case of MoVSbNbO, it allowed a determination of the relative Sb^{III}/Sb^{V} contents of the two main phases of the complex catalysts. The results obtained in the latter case were consistent with X-ray absorption near-edge spectra (*174*).

A.5. *Catalysts Containing other Elements*

Other characterization of catalysts have dealt with isotopes such as ^{125}Te, ^{193}Ir, ^{99}Ru and ^{51}Eu. The tellurium-containing catalysts were MoVTeNbO ammoxidation catalysts (*175*) and Te-doped Cr_2O_3 hydration–dehydration catalysts (*176*) and the

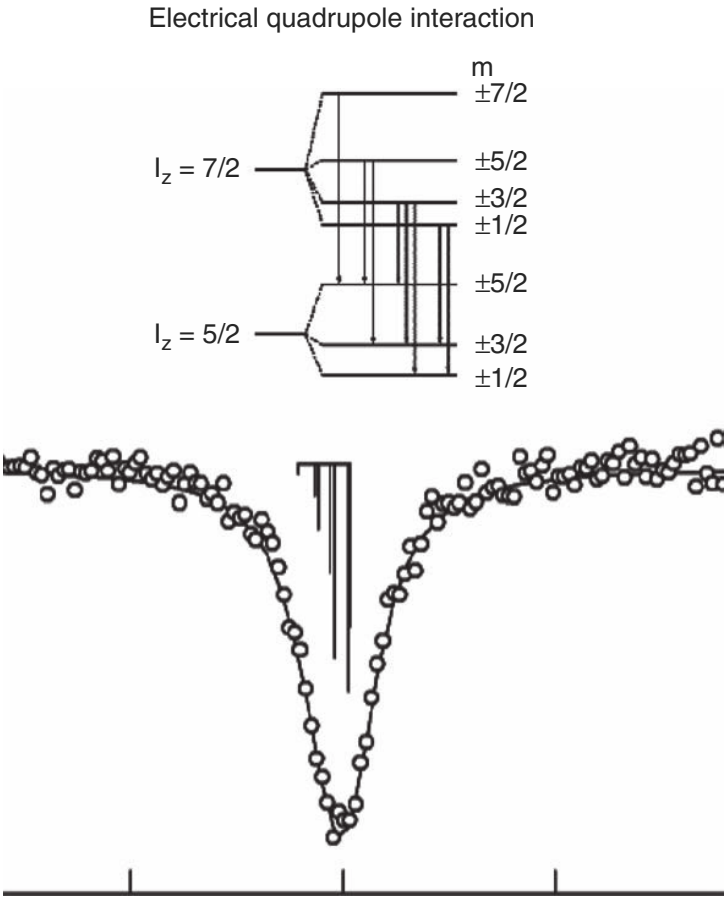

FIG. 9. Schematic representation of the electrical quadrupolar splitting in the case of a transition 5/2→7/2 like that of ^{121}Sb and corresponding the experimental spectra of FeSbO catalysts (*173*).

iridium-containing catalysts, iridium/iron bimetallic methanol synthesis catalysts (*177*); ^{99}Ru and ^{51}Eu spectroscopies were applied for the characterization of carbon-supported ruthenium–tin catalysts (used for the reduction of α,β-unsaturated aldehydes) (*178*) and the study of the hydrogen reduction of supported europium catalysts (*179*). These investigations are scarce, and all the published data have been cited here to illustrate the breadth of the applications of Mössbauer spectroscopy.

B. Investigations of Catalysts in Reactive Atmospheres and under Working Conditions

Characterization of catalysts in reactive atmospheres and during catalysis has led to insights that have not emerged from other characterizations. The introduction of EMS (^{57}Co) to investigate Co–Mo/Al_2O_3 hydrodesulfurization catalysts in reactive atmospheres was a key technological advance in the 1980s; it provided the first detailed insight into the nature of the promoter atoms in the active sulfided state of the catalysts and showed that the catalytic activity was related to the presence of the Co–Mo–S edge structures (*10,11*).

Since that time, Mössbauer spectroscopy has been used widely to characterize catalysts in reactive atmospheres, leading to continuous progress in the understanding of structure/catalytic property relationships (*180–194*).

Methodologies for investigation of solid catalysts under real working conditions with simultaneous measurements of catalytic activity data have advanced markedly in recent years, and Mössbauer spectroscopy has played an important role. Only isotopes that can be investigated at room temperature or higher temperatures (^{57}Fe,^{57}Co, ^{119}Sn, and ^{151}Eu) have been used in this context; they are powerful because they allow the characterization of the local atomic environment of the working catalytic species, giving rise to unique fingerprints of the catalytic sites.

It is important in this section to differentiate between the catalyst characterizations with Mössbauer spectroscopy under real working conditions and those performed under controlled environments after quenching of the reaction. Only recently (in the preceding 1–2 years) has this distinction been made with some clarity; the unclear term "*in situ*" has been used often in the literature for both types of investigations; the reader should be aware of this issue and carefully review the experimental conditions when the term "*in-situ*" is used.

B.1. *Investigations of Functioning Catalysts*

Investigations of functioning catalysts with Mössbauer spectroscopy have been performed for a wide range of samples and applications. The reactions include hydrodesulfuration (*15*), the Fischer–Tropsch reaction (*20,180*), selective oxidation or oxidative dehydrogenation (*181–186*), and acetonitrile synthesis (*187*).

We have seen in the first part of this article that the time required for obtaining a Mössbauer spectrum is rather long. The application of the technique to follow time-dependent changes has been limited, and in most cases it is catalysts operating under steady-state conditions that have been characterized. A great advantage of Mössbauer spectroscopy is that the measurements can be done under extreme working conditions, at both, high pressures and high temperatures. This essential point, which sets Mössbauer spectroscopy apart from numerous other methods for characterization of catalysts, is illustrated by the example of an industrial cobalt-containing Fischer–Tropsch catalyst investigated by ^{57}Co Mössbauer emission spectroscopy (*24*). A cell has been constructed that allows investigation of catalysts at temperatures up to 723 K and pressures up to 20 bar with injection of steam at 10 bar, permitting the production of wax and continuous catalyst test runs lasting up to 2 months (Fig. 10). The stainless steel cell is composed of two compartments. The inner one which corresponds to the high temperature and high pressure reactor and the outer one which is there to safely confine the radioactive ^{57}Co in case the inner one fails. The thickness of the beryllium windows of the two compartments have been optimized to support high pressure without absorbing too much γ-rays. The catalyst is placed onto a sintered metal filter with pore size diameter of 5 μm that allows the reactive gas to flow from top to bottom through the catalyst powder. This filter also allows draining of the produced wax downwards in a specially designed reservoir. It is stressed that only few physical chemical techniques can be used under such drastic conditions.

To investigate the deactivation of these catalysts, a ^{57}Co-containing catalyst was prepared by adding *ca.* 1000 ppm of ^{57}Co to a cobalt and platinum supported on

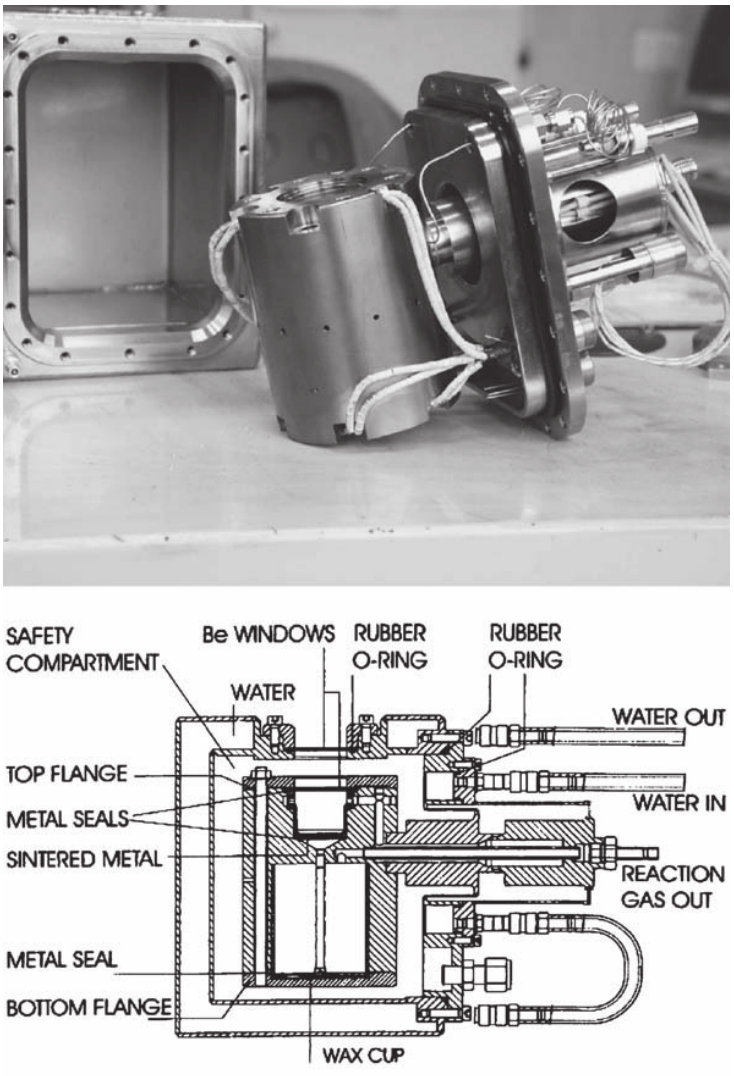

FIG. 10. Photograph and schematic representation of high-pressure Mössbauer emission spectroscopy cell (*24*).

alumina catalyst. This catalyst, the initial composition of which was 15Co/0.025Pt/$100Al_2O_3$, was then reduced in hydrogen at 653 K for 16 h (*20*). The Mössbauer emission spectrum showed about 70% reduction of cobalt. The catalyst was subsequently treated at 423 K in the cell in a hydrogen–water gas mixture with $H_2/H_2O = 1$ (molar) at 1, 5, and 10 bar, corresponding to a water partial pressures of 0.5, 2.5, and 5 bar, respectively. The Mössbauer emission spectra showed that the amount of metallic cobalt increased from 70% at 1 bar to 86% at 10 bar total pressure. These results show that the catalysts resisted oxidation under the conditions used and became more and more reduced when the total pressure (and thus the water partial pressure) increased. The investigation also showed that water was not responsible for the deactivation of the cobalt-containing Fischer–Tropsch catalysts. It was inferred that the deactivation should better be described as a surface poisoning or a carbon deposition, as had been proposed (*188,189*).

With the same type of cell, it has recently been possible to investigate the sulfidation of calcined Co–Mo/Al_2O_3 hydrodesulfurization catalysts under

realistic hydrotreatment conditions, with an activation of the catalysts at 673 K and 40 bar (*20*).

In another example, a complex multi-component BiMoCoFeO catalyst used in the partial oxidation of propene to acrolein was characterized by Mössbauer spectroscopy. This example has been chosen because it provides a good demonstration of the high efficiency of Mössbauer spectroscopy for the characterization of working catalysts (*181,182*).

In this investigation, $Co_{1-x}Fe_xMoO_4$ as pure solid solutions and in mixtures with $Bi_2(MoO_4)_3$ were characterized at 688 K under the conditions of propene oxidation to acrolein (C_3H_6:O_2:N_2 = 1:1:5.6 (molar ratios) at atmospheric pressure). The mechanical mixture of the mixed iron and cobalt molybdate with the bismuth molybdate has been shown to be a good model for the industrial catalysts, since both selectivity to acrolein and propene conversion larger than 95% could be simultaneously achieved on such catalyst (*190*). The data showed that under catalytic reaction conditions, no reaction was taking place between the two solid phases, which remained stable except when iron loadings were high and $Fe_2(MoO_4)_3$ was formed. A comparison of the data obtained with the pure solid solution and the mixtures of phases showed that cobalt stabilized Fe^{2+} sites in the solid solution while $Bi_2(MoO_4)_3$ stabilized Fe^{3+} sites in the solid solution. The presence of both species was proposed to be a key to the mild oxidation of propene by creating a high electrical conductivity, which favors the electron exchange in the Mars–van Krevelen mechanism. Furthermore, because iron sites have different environments in α and β polymorphic forms of $Co_{1-x}Fe_xMoO_4$, it was possible to determine the relative ratio of the two forms under the conditions of the catalytic test. It was confirmed that the β-type solid solution was more efficient than the α-type. Because the former was preferentially formed at high iron contents, it has been suggested that an optimal content of iron was present, which was sufficiently high to stabilize the β-phase but not too high, preventing the formation of ferric molybdate.

B.2. *Investigations of Quenched Catalysts*

It is not always possible to record Mössbauer spectra under catalytic reaction conditions, and characterization with this technique sometimes requires that spectra be measured at room temperature or at cryogenic temperatures. The latter limitation pertains to investigations involving isotopes that, by their very nature, require low temperature and to iron when phases are superparamagnetic at room temperature or higher temperatures. Most of the work reported in this category concerns ^{57}Fe; however, some investigations have been reported that deal with the characterization of PtSn particles (with the isotope ^{119}Sn) used in the selective hydrogenation of crotonaldehyde (which occurs at 353 K), the oxidation of CO (which occurs at room temperature) or the dechlorination of 1,2-dichloroethane (which occurs at 473 K) (*191–193*). In these investigations the spectra were recorded at 77 K under the reactive atmosphere after rapid quenching.

It is noteworthy that Mössbauer spectroscopy applies not only to solid–gas reactions but also to solid–liquid reactions. It has been used, for example, to

characterize (at 77 K) active site heterogeneity in pyrolyzed carbon-supported iron porphyrin catalysts for the electrochemical reduction of oxygen (*194*).

C. Investigation of Chemisorption of Reactants and Molecular Probes

Heterogeneous catalysis results from interactions between molecules in a gas or liquid phase and active sites at the surface of a solid. Mössbauer spectroscopy, which is an elemental probe technique, may be used to investigate adsorption sites containing appropriate isotopes and thereby gain information about adsorption and reaction processes.

Several examples of chemisorption investigations with Mössbauer spectroscopy appeared in the literature of the 1980s (*2*). In contrast, only very few investigations were reported in recent years. This lack may be explained on the one hand by the development of other techniques such as infrared spectroscopy, which are better adapted, more reliable, and easier to perform than Mössbauer spectroscopy, and on the other by the difficulties of interpretation of Mössbauer spectra.

These difficulties have several origins. For example, *f* factors of surface species, especially in their component perpendicular to the surface, will change extensively as a result of the adsorption or desorption of molecules. In the case of carbon-supported Pt–Fe catalysts, the doublet corresponding to iron atoms at the surface of the alloy particles was detected only when hydrogen was adsorbed (*195*). In the case of small particles dispersed on a support, the discrimination of resonant species at the surface of the particles from bulk species is possible only if the former are sufficiently numerous compared to the latter. This requirement implies a particle size that does not exceed about 20 nm. Furthermore, these surface species are not always easily differentiated from bulk species. The major parameter that allows such differentiation is the quadrupolar splitting which may strongly vary because of the larger electric field gradient related to the structural discontinuity at the surface. In the case of magnetic compounds, the hyperfine field at the surface has to be different from that in the bulk. Though agreement seems to have been reached on this point, it remains questionable in most cases whether the change may be detectable. Furthermore, it is often difficult to separate surface effects from size effects (such as superparamagnetism or collective magnetic excitations). Chemisorbed molecules have been shown to affect the total magnetic anisotropy constant of small particles and thus change their superparamagnetic relaxation times. Partial reconstruction of the surface may also occur and complicate the data analysis even more.

Among the few investigations reported on chemisorption of molecules, two are cited. Both concern N_2 chemisorption on FeZSM-5 (*196*) and on small αFe particles supported on carbon (*197*). In the first case, the affinity of nitrogen for certain ferrous centers after adsorption at 623 K was clearly evidenced. In the second case nitrogen was shown to react with surface iron atoms only at temperatures up to 700 K, resulting in a number of different types of environments for the latter depending upon the number of nitrogen atoms in their proximity. The other such investigations that have been reported deal with the adsorption of gases such as H_2, CO, and SO_2 (*198,199*).

There are reports of the use of iron species as probes (chemisorbed species) to characterize supports and their adsorption properties. Burger *et al.* (*200*) used Mössbauer spectroscopy to characterize submicroscopic droplets of Sn(IV) and Fe(III) complexes carried in an alkane/naphthalene mixture. The analysis of the Mössbauer parameters gave a qualitative picture regarding the solution structure inside the pores and the adsorption and wetting properties of the solid.

Pol'shina *et al.* (*201*) investigated the introduction of heteroatoms such as O or N into active carbons by measuring the adsorption of ferric ions. Analysis by Mössbauer spectroscopy allowed them to distinguish and quantify ferric ions that form surface complexes with O-containing groups (carboxylate complexes).

IV. Perspective

A. Current Developments and Applications

A.1. *Mössbauer Spectroscopy of Catalysts under Working Conditions*

The preceding several years have witnessed an evolution in Mössbauer investigations in catalysis toward investigations of catalysts under working conditions, consistent with a general trend in spectroscopic characterization of catalysts. The trend in spectroscopy of catalysts is toward extreme conditions of temperature and pressure. Mössbauer spectroscopy is well suited to such conditions.

The development is still at an early stage, and so far there has been no report illustrating the coupling of Mössbauer spectroscopy of a working catalyst with another technique, except for on-line gas chromatography for product analysis. There is a great interest in simultaneous catalyst characterization with complementary spectroscopic methods applied in ways that ensure that the data are all internally consistent. Mössbauer spectroscopy is expected to play a role in such combined investigations of catalysts under working conditions (*202*).

A.2. *Mössbauer Spectroscopy of Catalysts below 4.2K*

With the development of nanoscaled catalysts, several recent studies have pointed out the great interest of recording Mössbauer spectra below 4.2 K up to 0.055 K (*100,203,204*); it allowed the identification at the surface of various support such as mesoporous silica or ZrO_2, the formation of nanometric iron oxide clusters; this identification was not possible in classical low temperature studies conducted above 4.2 K, which concluded to the presence of larger particles. The analysis by Mössbauer spectroscopy performed at lower temperature enabled to show that these larger particles were agglomerates of nanometric iron clusters and allowed to reach another level of resolution of ferric particles structures (*204*).

A.3. *Technological Advances and Theoretical Evaluation of Mössbauer Parameters*

In the preceding decade there have been no drastic changes in the design of Mössbauer spectrometers. However, two new innovations have recently been

proposed that both reduce the acquisition time and improve the precision of the measurements (*205,206*).

One of the problems of the conventional method of Mössbauer spectroscopy is the occurrence of pulse overlapping at high-count rates. The single channel analyzer (SCA) that is generally used to register pulses of the signal almost always records interfering noise pulses. Such pulse overlapping disturbs the amplitude spectrum, reduces the signal-to-noise ratio, and limits the maximum count rate of the data acquisition system, thereby increasing the duration of an experiment.

To solve this problem, new instrumentation has been proposed that includes a fast analog-to-digital converter (ADC) together with a modern digital signal processor, which significantly increases the count rate as a consequence of the elimination of pulse overlapping (*205*). The proposed instrumentation allows calculation of the exact amplitude of each pulse, which may be combined with the current velocity discrimination, therefore leading to the recording of a two-dimensional Mössbauer spectrum (Fig. 11). The application of such two-dimensional data acquisition systems allows one to choose the optimal energy window in the amplitude spectrum after the experiment and to measure γ-quanta absorption and X-ray emission spectra simultaneously in the same transmission experiment. The new instruments also reduce data acquisition time, because amplitude and Mössbauer spectra are collected simultaneously.

Even more interesting is a new spectrometer that has been built with a novel moving system that synchronizes the movement of the radioactive source with that of the detector (*206*). This system allows the accumulation of Mössbauer spectra either in constant acceleration or constant velocity modes, therefore giving better signal-to-noise ratios and also reducing the time necessary for accumulation of a spectrum. Narrower line widths were also obtained with this equipment design.

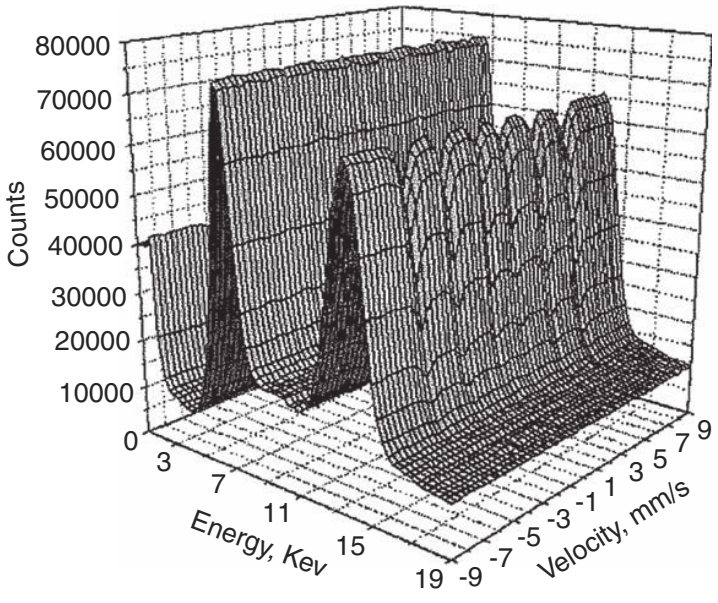

FIG. 11. Two-dimensional Mössbauer spectrum of an iron foil, measured with a proportional counter. Figure according to Maltsev *et al.* (*205*).

Furthermore, the theoretical evaluation of the Mössbauer hyperfine parameters (isomer shift (*IS*), quadrupolar splitting (*QS*), and magnetic hyperfine field (*H*)) is now possible with first-principles electronic structure calculations based on density functional theory (DFT) (*207,208*). The quality of the data depends on the size of the atomic cluster chosen to represent the solid and the charge densities around the nucleus under investigation. A detailed understanding of the relationships between the electrical field gradient or magnetic field and their various causes can come only from comparisons with sufficiently complete electronic structure calculations. Such calculations for realistic local and longer-range environments are rare and are very much needed, especially for the characterization of surface species.

A.4. *Mössbauer Spectroscopy and High-Throughput Catalyst Characterization*

The implementation of combinatorial chemistry and automated methods for rapid synthesis, testing, and characterization of catalysts, has opened a wide range of new opportunities in catalysis. However, so far, Mössbauer spectroscopy has not been introduced into this methodology. Two hurdles must be overcome for Mössbauer spectroscopy to become important in high-throughput catalyst characterization: the system for recording spectra must be scaled down, and the data acquisition and exploitation systems must be adapted.

The first condition could easily be fulfilled if progress made in spatial resolution were exploited. For example, an instrument has been developed that allows the measurement of Mössbauer spectra of metallurgical slags with a spatial resolution of approximately 500 μm (*209,210*). By use of a ^{57}Co source with high-specific activity, the γ-ray beam can be collimated from the conventional diameter of approximately 1 cm to a diameter of 500 μm. The sample is mounted in an epoxy resin, ground to a thin disk, and then mounted on an x–y stage directly behind a lead shield with a 500 μm hole. This technology should be easily applied to a sample set such as those generated with synthesis robots.

With regard to the second condition, advances in Mössbauer data analysis have progressed so far that it is currently possible to handle the fitting processes of a Mössbauer spectrum in a completely automated manner by using genetic algorithms and fuzzy logic; both software and hardware have been developed (*211,212*). Nevertheless, it is not trivial in many cases to relate the extracted hyperfine parameters to the underlying structure and properties of the material without a significant amount of experience, and many pitfalls have been documented (*213*).

The development of such integrated approaches to spectral analysis will benefit greatly from the large data bases and reference banks developed with the Mössbauer Effect Data Indexes covering 1958–1976 and the *Mössbauer Effect Reference and Data Journal* database (MERDJ: Vols. 1–19) covering 1976 to the present (http://www.unca.edu/medc/Journal.html).

A.5. *Mössbauer Spectroscopy for Characterization of Membranes and Monoliths*

Another advantage of Mössbauer spectroscopy that should benefit future research is that it can be used in a non-destructive way. This advantage should allow the investigation of membranes and monoliths without them being damaged, even

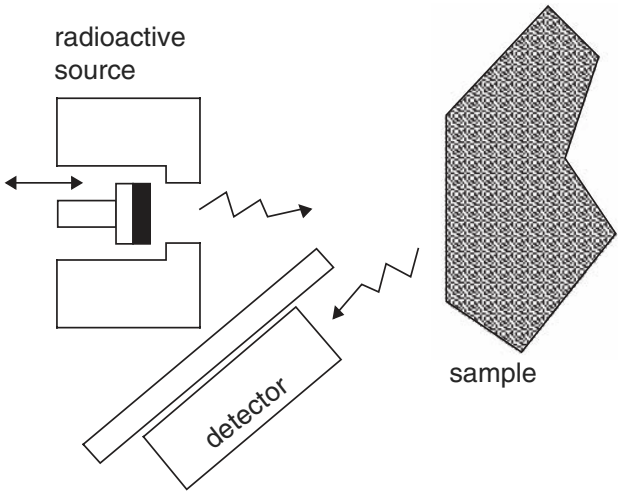

FIG. 12. Basic equipment for measuring a Mössbauer spectrum in diffusion mode.

under catalytic reaction conditions. This application can be achieved by experiments in the scattering or diffusion mode (Fig. 12). Furthermore, local micro heterogeneities in a monolithic or membrane sample may be characterized by use of an imaging Mössbauer spectroscopic device system (IMS), which can record 256 simultaneous Mössbauer spectra along a sample. The experimental system, which has been applied for the characterization of metallic ribbons, is based on a linear position-sensitive proportional counter that facilitates measurements with a spatial resolution on a length of about 50 μm (*214*).

Other improvements in spatial resolution in the future should allow more accurate investigation of conventional powdered samples such as catalysts. This will likely be made possible as a result of developments in synchrotron investigations of nuclear forward scattering (presented in the next section) (*215*). The development of a Mössbauer electron microscope that would focus conversion electrons using conventional electron optics has also been mentioned (*216*).

B. Future Developments and Applications

The main future developments of Mössbauer spectroscopy will undoubtedly be based on the use of synchrotron radiation as a source for Mössbauer experiments, taking advantage of its high flux, brilliance, pulse structure, and energy tunability. In the field of catalysis, new experimental opportunities include the use of parentless Mössbauer isotopes and time resolution. Catalyst characterizations should be possible over a wide range of time scales, including investigations of activation and deactivation under working conditions on time scales of tens to hundreds of seconds, investigations of transport processes such as diffusion on time scales from micro- to picoseconds, and investigations of processes such as relaxation and electron transfers on the intrinsic lifetime scale of the Mössbauer nuclei.

All these techniques are referred to as nuclear resonance scattering (NRS) of synchrotron radiation; they include a wide spectrum of experimental techniques, such as nuclear forward scattering (NFS), nuclear inelastic scattering (NIS), nuclear

Bragg diffraction (NBD), nuclear small-angle scattering (NSAS), nuclear reflectometry (NR), nuclear quasi-elastic scattering (NQES), and quasi-elastic and inelastic scattering with nuclear resonance energy analysis (*217*). In this review, we focus only on NFS and NIS, which are the two main techniques, and we attempt to describe the advantages of using them for the characterization of solid catalysts.

B.1. *Nuclear Forward Scattering (NFS) of Synchrotron Radiation*

Synchrotrons produce photons with energies in the range of nuclear Mössbauer transitions and can, in principle, be used to excite these transitions. However, synchrotron radiation can be monochromatized to only about 1 meV with new monochromators. Because the accessible nuclear levels are extremely narrow (between 10^{-9} and 10^{-8} eV), it is only about 10^{-3} of the incident photons that can excite the nuclear levels (excitation cross-section could be as much as 10^3 Γ_0). This is far weaker than radiation that is non-resonantly scattered by the electronic processes in the solid arising from the scattering of the entire 1 meV width of the incident radiation.

This limitation has been overcome by use of the property of synchrotron radiation that can be emitted from electron clouds (bunches) circulating in the storage rings. Bunches are a few centimeters in length, corresponding to ~100 ps, and the time between two successive pulses is 2.8 ns to 2.8 μs (at the European synchrotron radiation facility). When a material absorbs X-rays, resonant and non-resonant scattering occurs. However, because of the lifetime of the nuclear excited state, the resonant scattering is delayed with respect to the non-resonant scattering (the natural lifetime of the first nuclear excited state for ^{57}Fe is 141 ns). By suppressing data acquisition during the short non-resonant pulses, it is possible to measure only the nuclear forward scattered intensity.

A typical NFS experiment may be described as follows (*218*): the pulsed synchrotron radiation impinges on the sample as bunches, as they are produced in the storage ring (Fig. 13a). The typical pulse duration is ~100 ps, and the period of pulse repetition is of the order of 200 ns, corresponding to the electron bunch distance. A fast detector records the transmitted and forward scattered radiation, and the time evolution of this intensity is used to discriminate the resonant from the non-resonant intensity (Fig. 13b). The black spikes corresponding to the exciting pulses, which define the "time zero" of the nuclear excitation are suppressed by a gating acquisition system in the course of the experiment. The signal between these spikes represents the nuclear forward scattered intensity that is recorded and which is delayed with respect to the exciting pulse as a consequence of the lifetime of the nuclear excited states.

Figure 14 shows three ^{57}Fe case studies of the time behavior of the photons reemitted in the forward direction and a comparison with the typical spectra obtained in Mössbauer spectroscopy. Figure 14a corresponds to the case for which there is no hyperfine interaction. The nuclear levels are not split, and only one transition between ground and excited state is possible. In that case, the Mössbauer spectrum shows a single-absorption line and contains only γ-quanta of equal energy. In the presence of an electric field gradient (Fig. 14b), the splitting of the excited state is

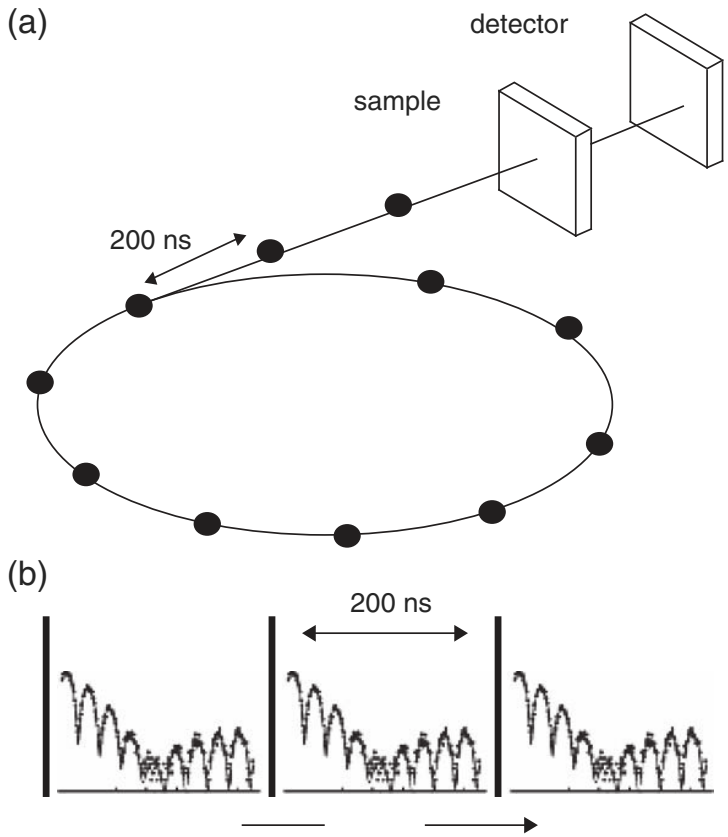

FIG. 13. Basic equipment for an NFS experiment (a) and time structure of the detected radiation (b).

observed, and the Mössbauer spectrum has two absorption lines (a doublet). Accordingly, the NFS spectrum shows characteristic modulations caused by the interference of the two forward re-emitted radiations containing γ-quanta with two different energies (quantum beats). The equal probability of the two transitions is directly evidenced by the symmetry of the doublet and is evaluated on the basis of the contrast between the maximum and the minimum of the beats. This contrast vanishes with increasing inequality of the two probabilities.

When a magnetic hyperfine field is present (Fig. 14c), both ground and excited states split into sub-levels, which leads to the observation of six absorption lines corresponding to the six transitions allowed by selection rules (sextet) in the Mössbauer spectrum. In the NFS spectrum, these transitions give rise to interferences and the superposition of quantum beats of different frequencies. The latter superposition leads to complex patterns that are difficult to interpret. In that case, the intrinsic polarization of the incident synchrotron radiation (the radiation is linearly polarized in the plane of the synchrotron ring) may advantageously be used to reduce the number of free parameters (i.e., to reduce the number of hyperfine radiation components and consequently reduce the number of quantum beats). The polarization of the synchrotron radiation mentioned above is an important property of the source, which is different from the source used for conventional Mössbauer experiments, because radioactive sources emit non-polarized radiation. The mechanism producing synchrotron radiation guarantees almost complete linear

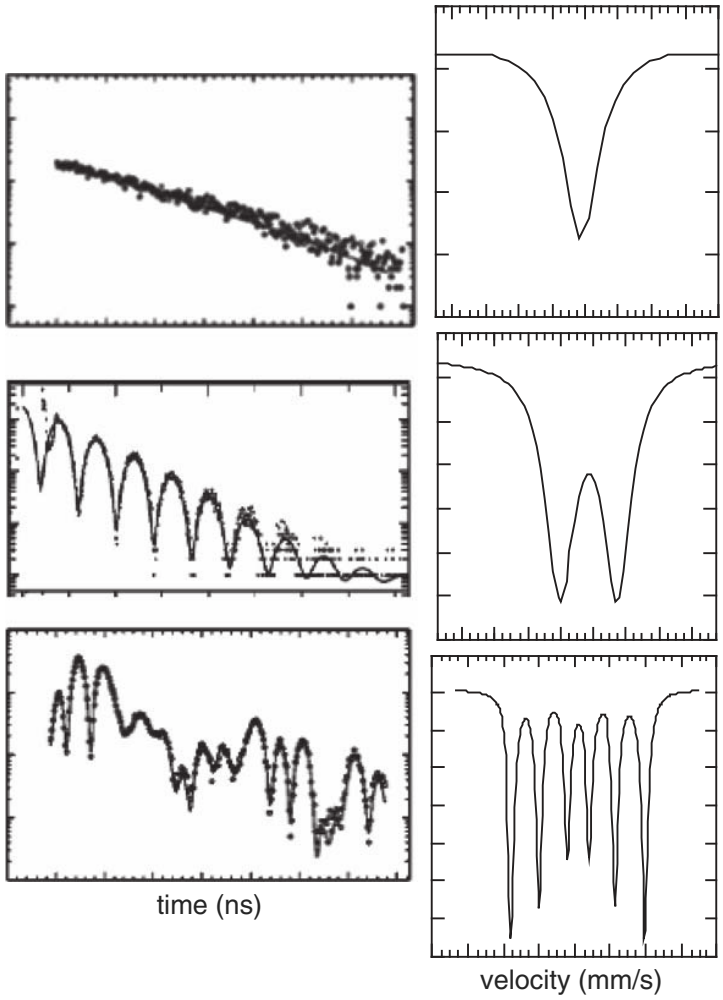

FIG. 14. Examples of experimental NFS time patterns with corresponding schematic conventional Mössbauer spectra: (a) stainless steel (*221*), (b) iron porphyrin complex $[Fe(CH_3COO)(TP_{piv}P]^-$ (spectrum taken at 30 K in a 4 T field) (*222*), and (c) α-Fe (*221*).

polarization. Furthermore, optical elements can convert synchrotron radiation into circularly polarized radiation with high efficiency.

When experimental NFS spectra of samples with finite thickness are recorded, the time decay also shows modulations attributed to coherent multiple scattering occurring in solids (dynamical beats). These superimposed modulations have different (non-periodic) time modulation and are taken into account when the spectra are fitted.

At this point, if we consider the Mössbauer parameters calculated in conventional Mössbauer spectroscopy, the isomer shift (*IS*) is not accessible from NFS spectra, because the latter only shows interference between radiation fields corresponding to different radiations. Isomer shifts will have to be measured relative to a second reference absorber that must be placed behind or in front of the sample along the γ-ray beam.

When the nuclei are subjected to an electrical quadrupole interaction, the NFS pattern shows quantum beats with a single frequency corresponding to the energy difference between the sub-levels of the exited state (ΔE_Q), which is equal to the

quadrupolar splitting (Δ). The time dependence of the intensity of the delayed radiation can be expressed approximately as follows:

$$I(t) \approx \exp\left(-\frac{t}{\tau}\right)\cos^2\left(\frac{\Delta E_Q t}{2\hbar}\right), \tag{20}$$

where τ is the natural lifetime of the nuclear transition ($\tau = 141$ ns for ^{57}Fe). This expression contains two time-dependent terms. The first, $\exp(-t/\tau)$, corresponds to the nuclear decay and the second, $\cos^2(\Delta E_Q t/2\hbar)$, to the quantum beat pattern; ΔE_Q, which is equal to $h2\pi/F$ (F is the period of the quantum beats), can be estimated using the following approximate relationship:

$$\Delta E_Q[mm/s]F[ns] \approx 87. \tag{21}$$

For magnetic compounds, the determination of the internal magnetic field requires the decomposition of the complex spectra of multi-quantum beats. Computer codes now allow one to attempt to perform such decomposition and to interpret the spectra. The determination of the complex quantum beat structure requires spectra recorded over long periods for high accuracy. In spite of that, analysis of complex spectra remains very often difficult and NFS does not compete against conventional Mössbauer spectroscopy. However, it offers a major advantage over the latter technique by being a time-resolved technique, with accumulation times in the range of minutes or less. This advantage is gained without loss of the advantages of the Mössbauer technique, such as site selectivity, quantitative analysis, and applicability to catalysts under extreme working conditions (high pressure and high temperature). The NFS technique benefits from the outstanding properties of synchrotron radiation, such as the high collimation of the photon beam that prevents Mössbauer line asymmetry resulting from the finite dimensions of the source. Furthermore, it can easily be combined with several complementary spectroscopic techniques.

As in conventional Mössbauer spectroscopy, ^{57}Fe is the most widely used isotope in nuclear resonant scattering of synchrotron radiation. Experiments with other isotopes, such as ^{169}Tm, ^{119}Sn, ^{83}Kr, ^{181}Ta, ^{151}Eu, ^{161}Dy, and ^{149}Sm have been reviewed recently (*219*). Other isotopes with very short half-life time sources should also be usable. The applicability of such isotopes represents another strong advantage that can be exploited in the future for catalyst characterization. The investigation of isotopes such as ^{197}Au ($E_\gamma = 77.34$ keV; source, ^{197}Pt, half-life, 18 h); ^{61}Ni ($E_\gamma = 67.40$ keV; source, ^{61}Co, half-life, 99 min); ^{186}W ($E_\gamma = 122.5$ keV; source, ^{186}Re, half-life, 90 h); ^{99}Ru ($E_\gamma = 89.36$ keV; source, ^{99}Rh, half-life, 16 days); or ^{125}Te ($E_\gamma = 35.46$ keV; source, ^{125}I, half-life, 60 days) may be expected.

As was stated in Section II.A, the energy resolution of the radioactive sources used in conventional Mössbauer spectroscopy is typically 10^{-9} eV. This resolution is determined by the natural line width and the maximum energy range obtained by Doppler-shifting techniques. In the case of synchrotron radiation, the energy resolution, which is related to the time period following the excitation of the isotope, is superior to that in conventional Mössbauer spectroscopy. This period can be as short as 2.8 μs, which leads to an energy resolution of about 10^{-10} eV. However, the

recordable period is determined by the bunch separation, which depends on the operationing mode of the synchrotron. The energy resolution, which depends on this period, will be superior to that of the radioactive source only if the bunch separation is larger than the lifetime of the excited nuclear state. The reported examples of experimental characterization of solids mainly concern biological inorganic solids (*220*) or geological samples (*221*). In the latter case, the measurements were made at pressures up to 1.5 Mbar.

B.2. *Nuclear Inelastic Scattering (NIS) of Synchrotron Radiation*

This technique comprises measurement of the energy distribution of phonons excited by the inelastic absorption of X-rays at the resonance. The Mössbauer effect comprises the absorption and re-emission of X-rays that occur in an elastic manner. This excitation can also be achieved if the radiation energy is not exactly equal to the resonance energy E_0, but instead is equal to $E_0 \pm \Delta E$ when a phonon of energy ΔE is annihilated providing the lacking energy or a phonon of energy ΔE is created, taking up the excess energy. Annihilation or emission of several phonons can be involved in the process. When resonance absorption takes place with detuned synchrotron radiation, the delayed re-emitted γ-quanta or conversion electrons are emitted into a solid angle of 4π and can be counted by a detector placed at a position out of the incoming beam (Fig. 15).

The normalized probability of nuclear inelastic absorption $W(E)$ can be decomposed in terms of a multi-phonon expansion (*222,223*):

$$W(E) = f\left(\delta(E) + \sum_{np=1}^{\infty} S_{np}(E)\right), \tag{22}$$

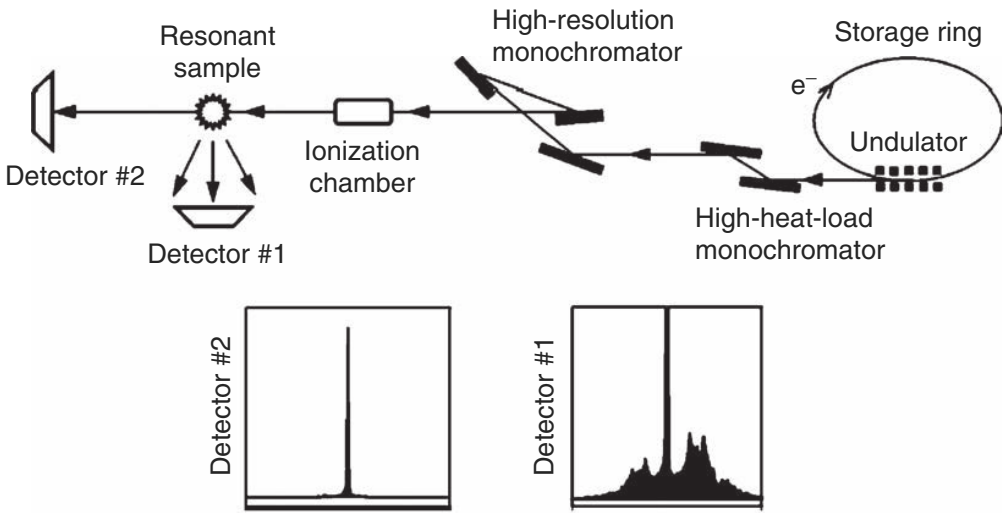

FIG. 15. Basic equipment for measuring a nuclear inelastic scattering spectrum. Detector 1 measures the intensity of the incoherent nuclear forward scattering, which proceeds both elastically and inelastically; detector 2 measures only the intensity of the coherent nuclear forward scattering, which proceeds elastically. Figure according to Rüffer and Chumakov (*224*).

where f is the Lamb–Mössbauer factor, $\delta(E)$ a Dirac function describing the elastic part of absorption (zero phonon term) and $S_{np}(E)$ a series of terms from which the npth term represents the inelastic absorption accompanied by creation - (annihilation) of np phonons. The one phonon term is given by

$$S_1(E) = \frac{E_R g(|E|)}{E(1 - e^{-\beta E})} \tag{23}$$

and the subsequent terms by the following when the harmonic approximation is valid:

$$S_1(E) = \frac{1}{np} \int_{-\infty}^{+\infty} S_1(E') S_{np-1}(E - E')\, dE'. \tag{24}$$

In these expressions, $\beta = (kT)^{-1}$; $E_R = \hbar^2 k^2 / 2M$is the recoil energy of a free nucleus; k the wave vector of the γ-ray quantum and M the mass of the nucleus. The function $g(E)$ is the normalized density of phonon states:

$$g(E) = V_0 \frac{1}{(2\pi)^3} \sum_j \int d\vec{q} \delta\left[E - \hbar\omega_j(\vec{q})\right], \tag{25}$$

where V_0 is the volume of the unit cell, and the index j enumerates the branches of the dispersion relation $[\hbar\omega_j(\vec{q})]$ with $\vec{q}$ being the phonon momentum. The integral is taken within the first Brillouin zone.

This technique, besides allowing determination of the Lamb–Mössbauer factor, provides direct access to the density of phonon states for the probe isotope in a solid. It thus provides information about lattice dynamics that is excluded by the limitations of Mössbauer spectroscopy. This technique could be valuable in investigations of adsorption with the adsorbing element as the probe and showing the modifications brought about by the adsorbate on the dynamic properties of the probe.

The frequency distribution of vibrations can be different in various directions, although Mössbauer spectroscopy did not show it (*225*). Few examples are available to illustrate the use of the technique. Furthermore, most of these examples have been chosen to show basic applications of the technique. Temperature and pressure dependences of nuclear inelastic absorption in iron metal (α-Fe) have been investigated (*226*), as has the anisotropy dependence in a $^{57}FeBO_3$ single crystal (*225*). NIS has also been used to investigate complexes in solution (^{57}Fe[2,2′-(bipyridyl)$_3$]Cl$_2$ in water and in glycerol) (*227*). A recent publication reports the characterization of perovskite-related oxides ((Sr,Ca)(Fe,Co)$O_{3-\delta}$ and (Ba,Ca)(FeCo)$O_{3-\delta}$) that may find applications in fuel cells or oxygen-permeable membranes (*228*). In the latter case, a soft phonon peak in the NIS spectra was found to be correlated with oxygen ordering in the structure. Changes were also observed upon absorption of CO_2 that have unfortunately not been interpreted because of the complexity of the spectra.

Nuclear resonant forward scattering and inelastic scattering of synchrotron radiation constitute a promising field for development of catalyst characterization in the future. For the characterization of solid catalysts, NFS has the advantage over

Mössbauer spectroscopy of being a time-resolved spectroscopic technique. This characteristic opens new areas of research, particularly because it also combines in the same time all the advantages of Mössbauer spectroscopy in terms of sensitivity (it is even more sensitive for hyperfine parameter effects than conventional Mössbauer spectroscopy) and in terms of applicability under catalytic reaction conditions. It still appears, however, for complex systems, such as those often encountered in catalysis, difficult to analyze the time-domain spectra relative to energy-domain spectra, and for the time being NFS should be considered to be complementary to conventional Mössbauer spectroscopy and not a replacement of it. In the future, NIS may also become an extremely efficient tool for characterizing adsorption, although the energy resolution for recording molecular vibrations, which is at present time about $5\,cm^{-1}$, has to be improved.

V. Conclusions

This review includes a short summary of the principles of Mössbauer spectroscopy and of recent applications of the technique in heterogeneous catalysis. The frequency of applications of the technique in this field has remained nearly constant, but the applications to investigations of catalysts under controlled conditions and under catalytic reaction conditions, with characterizations of activation, reaction, and deactivation processes has increased significantly in the preceding few years. Although Mössbauer spectroscopy is characterized by complexity in the experimental technique as well as in the interpretation and analysis of spectra, if offers for samples including those incorporating iron, cobalt, gold, and other elements of catalytic interest the capability for (i) determination of accurate oxidation states of the metals, (ii) resolution of microcrystalline or poorly crystalline phases, (iii) quantification of coordination and local symmetry site populations, (iv) characterization of various electronic, magnetic, and (v) structural phase transitions; and quantification of chemical, structural, and magnetic disorder.

A section of this review is devoted to the potential areas of likely future developments in Mössbauer spectroscopy in the field of catalysis. In view of the considerable value of spectroscopic measurements made of catalysts while they are working, Mössbauer spectroscopy, which is relatively well adaptable to such conditions, is expected to gain interest in the catalysis community. Cells have already been adapted to conditions of high pressure and high temperature. Furthermore, these cells provide flexibility, allowing the coupling of Mössbauer spectroscopy with other spectroscopic techniques. New experimental setups continue to be developed and should improve the precision of the measurements and reduce the acquisition time (which still remains a handicap for the technique). Synchrotron Mössbauer spectroscopy in particular deserves more attention because it can become a useful for investigating catalytic reactions on many types of catalysts. The use of synchrotron radiation for Mössbauer spectroscopy was proposed as early as 1974, and it is now becoming accessible to non-experts. NFS of synchrotron radiation allows experiments that are in many aspects very similar to conventional Mössbauer spectroscopy, and they offer the benefit of combining all the advantages of

conventional Mössbauer spectroscopy, with the time-resolution of NFS at a time scale interesting for catalyst characterizations. This latter advantage is conspicuously missing in conventional Mössbauer spectroscopy when compared with other spectroscopic techniques for characterizing catalysts under working conditions. In the future, NIS experiments may bring new insights in catalyst characterization, and these techniques should also broaden the field of application of Mössbauer spectroscopy to allow the investigation of important isotopes with very short half-lifetime sources, such as ^{61}Ni and ^{99}Ru.

It is hoped that the synthetic presentation of NFS and NIS techniques given in this review will trigger scientists' interest in exploring these new opportunities in catalyst characterization.

References

1. Popescu, A., Szabo, A., and Hobert, H., *Rev. Roum. Chim.* **16**, 869 (1971).
2. Dumesic, J.A., and Topsoe, H., *Adv. Catal.* **26**, 121 (1989).
3. Phillips, J., *Hyp. Interact.* **111**, 3 (1998).
4. van der Kraan, A.M., *Hyp. Interact.* **111**, 23 (1998).
5. Niemantsverdriet, J.W., *Stud. Surf. Sci. Catal.* **123**, 489 (1999).
6. van der Kraan, A.M., *Hyp. Interact.* **126**, 107 (2000).
7. Lippens, P.E., *Solid State Comm.* **113**, 399 (2000).
8. Naoufal, D., Millet, J.M.M., Garbowski, E., Brullé, Y., and Primet, M., *Catal. Lett.* **54**, 141 (1998).
9. Kündig, W., Bömmel, H., Constabaris, G., and Lindquist, R.H., *Phys. Rev.* **142**, 327 (1966).
10. Topsøe, H., Clausen, B.S., Candia, R., Wivel, C., and Mørup, S., *J. Catal.* **68**, 435 (1981).
11. Wivel, C., Candia, R., Clausen, B.S., Mørup, S., and Topsøe, H., *J. Catal.* **68**, 453 (1981).
12. Crajé, M.W.J., de Beer, V.H.J., van Veen, J.A.R., and van der Kraan, A.M., *in* "Hydrotreating Technology for Pollution Control, Chemical Industries Series." (M.L. Occelli and R.R. Chianelli, Eds.), Vol. 67, p. 95. Marcel Dekker, New York, 1996.
13. Crajé, M.W.J., de Beer, V.H.J., van Veen, J.A.R., and van der Kraan, A.M., *Chem. Ind.* **67**, 95(London) (1996).
14. Dugulan, A.I., Crajé, M.W.J., and Kearley, G.J., *J. Catal.* **229**, 276 (2005).
15. Vissenberg, M.J., de Bont, P.W., van Oers, E.M., de Haan, R.A., Boellaard, E., van der Kraan, A.M., de Beer, V.H.J., and van Santen, R.A., *Catal. Lett.* **40**, 25 (1996).
16. Adachi, M., Contescu, C., and Schwarz, J.A., *J. Catal.* **162**, 66 (1996).
17. Vissenberg, M.J., van der Meer, Y., Hensen, E.J.M., de Beer, V.H.J., van der Kraan, A.M., van Santen, R.A., and van Veen, J.A.R., *J. Catal.* **198**, 151 (2001).
18. van der Meer, Y., Vissenberg, M.J., de Beer, V.H.J., van Veen, J.A.R., and van der Kraan, A.M., *Hyp. Interact.* **139/140**, 51 (2002).
19. van der Meer, Y., Hensen, E.J.M., van Veen, J.A.R., and van der Kraan, A.M., *J. Catal.* **228**, 433 (2004).
20. Dugulan, A.I., Crajé, M.W.J., and Kearley, G.J., *J. Catal.* **222**, 281 (2004).
21. van de Loosdrecht, J., van Dillen, A.J., Reinders, D., van der Horst, A.A., Boellaard, E., van der Kraan, A.M., and Geus, J.W., *Stud. Surf. Sci. Catal.* **107**, 201 (1997).
22. van Berge, P.J., van de Loosdrecht, J., Barradas, S., and van der Kraan, A.M., *Prep. Am. Chem. Soc., Div. Pet. Chem.* **44**, 84 (1999).
23. van Berge, P.J., van de Loosdrecht, J., Barradas, S., and van der Kraan, A.M., *Catal. Today* **58**, 321 (2000).
24. Crajé, M.W.J., van der Kraan, A.M., van de Loosdrecht, J., and van Berge, P.J., *Catal. Today* **71**, 369 (2002).

25. van de Loosdrecht, J., van Berge, P.J., Craje, M.W.J., and van der Kraan, A.M., *Hyp. Interact.* **139/140**, 3 (2002).
26. Benaichouba, B., Bussiere, P., Coudurier, G., and Vedrine, J.C., *Hyp. Interact.* **69**, 743 (1991).
27. Gancedo, J.R., Gracia, M., and Marco, J.F., *NATO Sci. Ser. II: Math. Phys. Chem.* **94**, 41 (2003).
28. Kamzin, A.S., and Vcherashnii, D.B., *Tech. Phys. Lett.* **28**, 365 (2002).
29. O'Brien, R.J., and Davis, B.H., *Energy Fuels* **10**, 546 (1996).
30. Shroff, M.D., and Datye, A.K., *Catal. Lett.* **37**, 101 (1996).
31. Gallegos, N.G., Cagnoli, M.V., Bengoa, J.F., Alvarez, A.M., Yeramian, A.A., and Marchetti, S.G., *Stud. Surf. Sci. Catal.* **142A**, 525 (2002).
32. Ren, Q.Z., Zhang, Z.X., and Zhou, J.L., *J. Nat. Gas Chem.* **5**, 152 (1996).
33. Boellaard, E., van der Kraan, A.M., and Geus, J.W., *Appl. Catal. A* **147**, 22 (1996).
34. Shroff, M.D., Kalakkad, D.S., Harrington, M.S., Jackson, N.B., Coulter, K.E., Sault, A.G., and Datye, A.K., *Chem. Trans. Met. Carb. Nit.* **28**, 511 (1996).
35. Liu, Z.T., Li, Y.W., Zhou, J.L., Zhang, B.J., and Ping, J.Y., *Fuel Sci. Technol. Int.* **14**, 805 (1996).
36. Rao, K.R.P., Huggins, F.E., Huffman, G.P., Gormley, R.J., O'Brien, R.J., and Davis, B.H., *Energy Fuels* **10**, 546 (1996).
37. van Gruijthuijsen, L.M.P., Howsmon, G.J., Delgass, W.N., Koningsberger, D.C., van Santen, R.A., and Niemantsverdriet, J.W., *J. Catal.* **170**, 331 (1997).
38. van de Loosdrecht, J., van Dillen, A.J., Reinders, D., van der Horst, A.A., Boellaard, E., van der Kraan, A.M., and Geus, J.W., *Stud. Surf. Sci. Catal.* **107**, 201 (1997).
39. Boellaard, E., van der Kraan, A.M., Sommen, A.B.P., Hoebink, J.H.B., Marin, G.B., and Ge, J.W., *Appl. Catal. A* **179**, 175 (1999).
40. van Berge, P.J., van de Loosdrecht, J., Barradas, S., and van der Kraan, A.M., *Catal. Today* **58**, 321 (2000).
41. Meitzner, G.D., Hamdeh, H.H., Davis, B.H., and Iglesia, E., *Appl. Catal. A* **219**, 215 (2001).
42. Zhang, Y.Q., Sirimanothan, N., O'Brien, R.J., Hamdeh, H.H., and Davis, B.H., *Stud. Surf. Sci. Catal.* **139**, 125 (2001).
43. Li, S.Z., O'Brien, R.J., Meitzner, G.D., Hamdeh, H.H., Davis, B.H., and Iglesia, E., *Appl. Catal. A* **219**, 215 (2001).
44. Goossens, A.G., de Jongh, L.J., Butter, K., Philipse, A.P., Crajé, M.W.J., and van der Kraan, A.M., *Hyp. Interact.* **141/142**, 381 (2002).
45. Duvenhage, D.J., and Coville, N.J., *Appl. Catal. A* **233**, 63 (2002).
46. Alvarez, A.M., Bengoa, J.F., Cagnoli, M.V., Gallegos, N.G., Yeramián, A.A., and Marchetti, S.G., *Stud. Surf. Sci. Catal.* **142A**, 133 (2002).
47. Motjope, T.R., Dlamini, H.T., Hearne, G.R., and Coville, N.J., *Catal. Today* **71**, 335 (2002).
48. Yang, Y., Xiang, H.W., Xu, Y.Y., Bai, L., and Li, Y.W., *Appl. Catal. A* **266**, 181 (2004).
49. Duvenhage, D.J., and Coville, N.J., *Appl. Catal. A* **289**, 231 (2005).
50. Yang, Y., Xiang, H.W., Tian, L., Wang, H., Zhang, C.H., Tao, Z.C., Xu, Y.Y., Zhong, B., and Li, Y.W., *Appl. Catal. A* **284**, 105 (2005).
51. Jiang, K.Y., Yang, X.L., and Wu, Z., *Hyp. Interact.* **77**, 67 (1993).
52. Yang, X.L., Weng, S.H., Jiang, K.Y., Mao, L.S., Yuan, Y.T., and Jin, G.L., *Cuihua Xuebao* **14**, 27 (1993).
53. Parvulescu, V.I., Filoti, G., Parvulescu, V., Grecu, N., Angelescu, E., and Nicolescu, I.V., *J. Mol. Catal.* **89**, 267 (1994).
54. Jiang, K.Y., Yang, J.X., Hu, B.Y., Yang, X.L., Mao, L.S., Yuan, Y.T., and Zhang, G.L., *Hyp. Interact.* **111**, 45 (1998).
55. Zhu, Y., Feng, L., Chen, R., and Wang, J., *Huaxue Wuli Xuebao* **12**, 49 (1999).
56. Zhu, Y., Chen, R., Feng, L., and Wang, J., *Wuli Huaxue Xuebao* **15**, 234 (1999).
57. Jiang, K.Y., Yang, X.L., Yuan, Y.T., Mao, L.S., and Yang, D.P., *Hyp. Interact.* **139/140**, 97 (2002).
58. Kalenczuk, R.J., *Appl. Catal. A* **112**, 149 (1994).
59. Menon, P.G., and Kaugset, P.S., *Appl. Catal. A* **115**, 295 (1994).
60. Pattek-Janczyk, A., and Miczko, B., *Appl. Catal. A* **124**, 253 (1995).
61. Wang, W.X., Zhao, H.Q., Du, B.S., Wen, J.M., Li, F., and Wang, D.M., *Appl. Catal. A* **122**, 5 (1995).

62. Kalenczuk, R.J., *J. Chem. Tech. Biotechnol.* **64**, 398 (1995).
63. Pattek-Janczyk, A., *Appl. Catal. A* **124**, 267 (1995).
64. Kalenczuk, R.J., *Catal. Lett.* **33**, 255 (1995).
65. Pattek-Janczyk, A., Miczko, B., and Morawski, A.W., *Appl. Catal. A* **141**, 1 (1996).
66. Ostoshevskaya, O.Y., Serdyukov, S.I., and Fabritchnyi, P.B., *Kinet. Katal.* **6**, 931 (1996).
67. Li, X.N., Liu, H.Z., and Chen, S.Y., *Cuihua Xuebao* **19**, 201 (1998).
68. Jacobsen, C.J.H., Jiang, J.Z., Mørup, S., Clausen, B.S., and Topsoe, H., *Catal. Lett.* **61**, 115 (1999).
69. Pattek-Janczyk, A., Grenier, J.C., and Miczko, B., *Solid State Ionics* **117**, 95 (1999).
70. Kalenczuk, R.J., *Int. J. Inorg. Mater.* **2**, 233 (2000).
71. Vissokov, G.P., *Catal. Today* **72**, 197 (2002).
72. Mitov, I.G., and Andreev, A.A., *Bulg. Chem. Commun.* **30**, 82 (1998).
73. Koy, J., Ladebeck, J., and Hill, J.R., *Stud. Surf. Sci. Catal.* **119**, 479 (1998).
74. Favre, A., Guillaume, N., Millet, J.M.M., and Primet, M., *Catal. Lett.* **49**, 207 (1997).
75. Liu, Q., Ma, W., He, R., and Mu, Z., *Catal. Today* **106**, 52 (2005).
76. Mehner, H.W., Meisel, W.P.E., Bruckner, A., and York, A.P.E., *Hyp. Interact.* **111**, 51 (1998).
77. Alptekin, G.O., Herring, A.M., Williamson, D.L., Ohno, T.R., and McCormick, R.L., *J. Catal.* **181**, 104 (1999).
78. Sakaeva, N.S., Varnek, V.A., Bukhtiyarova, G.A., Anufrienko, V.F., Sobolev, E.A., and Zolotovskii, B.P., *React. Kinet. Catal. Lett.* **70**, 169 (2000).
79. Mitov, I.G., Dotcheva, D., Cherkezova-Zheleva, Z., and Mitrov, V.I., *NATO Sci. Ser., Ser. C* **546**, 383 (2000).
80. Ivanov, K., Mitov, I.G., and Krustev, S., *J. Alloys Compd.* **309**, 57 (2000).
81. Anshits, A.G., Kondratenko, E.V., Fomenko, E.V., Kovalev, A.M., Bajukov, O.A., Anshits, N.N., Sokol, E.V., Kochubey, D.I., Boronin, A.I., Salanov, A.N., and Koshcheev, S.V., *J. Mol. Catal. A* **158**, 209 (2000).
82. Artizzu-Duart, P., Millet, J.M.M., Guilhaume, N., Garbowski, E., and Primet, M., *Catal. Today* **59**, 136 (2000).
83. Ge, X., Wang, Y., Shen, J.Y., and Zhang, H.L., *Wuji Huaxue Xuebao* **16**, 79 (2000).
84. Langpape, M., and Millet, J.M.M., *Appl. Catal. A* **200**, 89 (2000).
85. Soares, A.P.V., Portela, M.F., Kiennemann, A., Hilaire, L., and Millet, J.M.M., *Appl. Catal. A* **206**, 221 (2001).
86. Homonnay, Z., Nomura, K., Hamakawa, S., Hayakawa, T., Juhász, G., Kuzmann, E., and Vértes, A., *Hyp. Interact.* **139/140**, 41 (2002).
87. Hodge, N.A., Kiely, C.J., Whyman, R.M., Siddiqui, R.H., utchings, G.J., Pankhurst, Q.A., Wagner, E., Rajaram, R.R., and Golunski, S.E., *Catal. Today* **72**, 133 (2002).
88. Jung, K.D., Joo, O.S., and Kim, C.S., *Catal. Lett.* **84**, 53 (2002).
89. Castelao-Dias, M., Costa, B.F.O., and Quinta-Ferreira, R.M., *Hyp. Interact.* **136**, 9 (2002).
90. Goldwasser, M.R., Dorantes, V.E., Perez Zurita, M.J., Sojo, P.R., Cubeiro, M.L., Pietri, E., González-Jiménez, F., Lee, Y.N., and Moronta, D., *J. Mol. Catal. A* **193**, 223 (2003).
91. Pankhurst, Q.A., Betteridge, S., Hargreaves, J.S.J., Joyner, R.W., Hutchings, G.J., and Taylor, S.H., *Conf. Proc. Ital. Phys. Soc.* **50**, 673 (1996).
92. Chen, K.D., Fan, Y.N., Hu, Z., and Yan, Q.J., *Catal. Lett.* **36**, 139 (1996).
93. Chen, K.D., Fan, Y.N., Hu, Z., and Yan, Q.J., *J. Solid State Chem.* **121**, 240 (1996).
94. Kalenczuk, R.J., *Int. J. Inorg. Mater.* **2**, 233 (2000).
95. Okamoto, Y., Kubota, T., Ohto, Y., and Nasu, S., *J. Catal.* **192**, 412 (2000).
96. Masuda, T., Kondo, Y., Miwa, M., Shimotori, T., Mukai, S.R., Okamoto, Y., Kubota, T., Ohto, Y., and Nasu, S., *J. Phys. Chem. B* **104**, 8462 (2000).
97. Suo, Z.H., Kou, Y., and Wang, H.L., *Cuihua Xuebao* **21**, 586 (2000).
98. Kubota, T., Ohto, Y., and Nasu, S., *J. Catal.* **192**, 412 (2000).
99. Okamoto, Y., Kubota, T., Ohto, Y., and Nasu, S., *J. Phys. Chem. B* **104**, 8462 (2000).
100. Millet, J.M.M., Signoretto, M., and Bonville, P, *Catal. Lett.* **64**, 135 (2000).
101. Hashimoto, K., Takano, M., Kawasaki, S., and Yoshida, S., *Chem. Eng. Sci.* **56**, 897 (2001).
102. Masuda, T., Kondo, Y., Miwa, M., Shimotori, T., Mukai, S.R., Hashimoto, K., Takano, M., Kawasaki, S., and Yoshida, S, *Chem. Eng. Sci.* **56**, 897 (2001).

103. van den Berg, F.R., Crajé, M.W.J., Kooyman, P.J., van der Kraan, A.M., and Geus, J.W., *Appl. Catal. A* **235**, 217 (2002).
104. van der Berg, F.R., Crajé, M.W.J., van der Kraan, A.M., and Geus, J.W., *Appl. Catal. A* **242**, 403 (2003).
105. Yang, J.X., Jiang, K.Y., Hu, B.Y., Yang, X.L., Mao, L.S., Yuan, Y.T., and Zhang, G.L., *Nucl. Sci. Tech.* **8**, 225 (1997).
106. Bond, G., Molloy, K.C., and Stone, F.S., *Solid State Ionics* **101**, 697 (1997).
107. Coquay, P., Peigney, A., de Grave, E., Vandenberghe, R.E., and Laurent, Ch., *J. Phys. Chem. B* **106**, 13199 (2002).
108. Benz, M., van der Kraan, A.M., and Prins, R., *Appl. Catal. A* **172**, 149 (1998).
109. Sanchez-Valente, J., Millet, J.M.M., Figueras, F., and Fournès, L., *Hyp. Interact.* **131**, 43 (2001).
110. Reshetenko, T.V., Avdeeva, L.B., Khassin, A.A., Kustova, G.N., Ushakov, V.A., Moroz, E.M., Shmakov, A.N., Kriventsov, V.V., Kochubey, D.I., Pavlyukhin, Y.T., Chuvilin, A.L., and Ismagilov, Z.R., *Appl. Catal. A* **268**, 127 (2004).
111. Arena, F., Gatti, G., Martra, G., Coluccia, S., Stievano, L., Spadaro, L., Famulari, P., and Parmaliana, A., *J. Catal.* **23**, 365 (2005).
112. Chen, K.D., Fan, Y.N., Hu, Z., and Yan, Q.J., *J. Solid State Chem.* **121**, 240 (1996).
113. Knops-Gerrits, P.P., van Bavel, A.M., Langouche, G., and Jacobs, P.A., *in* "Catalytic Activation and Functionalisation of Light Alkanes." (E.G. Derouane, J. Haber, F. Lemos, F. Ramoa Ribeiro and M. Guisnet, Eds.), Vol. 44, p. 215. Kluwer Academic Publishers, Dordrecht, Boston, London, 1998.
114. Coq, B., Mauvezin, M., Delahay, G., Butet, J.B., and Kieger, S., *Appl. Catal. B* **27**, 193 (2000).
115. Coq, B., Mauvezin, M., Delahay, G., and Kieger, S., *J. Catal.* **195**, 298 (2000).
116. Giordano, G., Katovic, A., Perathoner, S., Pino, F., Centi, G., Nagy, J.B., Lázár, K., and Fejes, P., *Stud. Surf. Sci. Catal.* **142**, 477 (2002).
117. Wang, X.D., Zhao, X.Q., Shen, J.Y., Sun, X.Y., Zhang, T., and Lin, L.W., *Phys. Chem. Chem. Phys.* **4**, 2846 (2002).
118. Taboada, J.B., Overweg, A.R., Kooyman, P.J., Arends, I.W.C.E., and Mul, G., *J. Catal.* **231**, 56 (2005).
119. Hall, W.K., Feng, X.B., Dumesic, J.A., and Watwe, R., *Catal. Lett.* **52**, 13 (1998).
120. Ovanesyan, N.S., Dubkov, K.A., Pyalling, A.A., and Shteinman, A.A., *J. Radioanal. Nucl. Chem.* **246**, 149 (2000).
121. Batista, M.S., Morales Torres, M.A., Baggio-Saitovitch, E.M., and Urquieta-Gonzalez, E.A., *Hyp. Interact.* **134**, 161 (2001).
122. Urquieta-González, E.A., Martins, L., Peguin, R.P.S., and Batista, M.S., *Mater. Res. (Sao Carlos, Braz.)* **5**, 321 (2002).
123. Heinrich, F., Schmidt, C., Löffler, E., Menzel, M., and Grünert, W., *J. Catal.* **212**, 157 (2002).
124. Fejes, P., Lázár, K., Marsi, I., Rockenbauer, A., Korecz, L., Nagy, J.B., Perathoner, S., and Centi, G., *Appl. Catal. A* **252**, 75 (2003).
125. Tuel, A., Arcon, I., and Millet, J.M.M., *Faraday Trans.* **94**, 3501 (1998).
126. Marchetti, S.G., Cagnoli, M.V., Alvarez, A.M., Bengoa, J.F., Gallegos, N.G., Yeramián, A.A., and Mercader, R.C., *Hyp. Interact.* **139/140**, 33 (2002).
127. Samanta, S., Giri, S., Sastry, P.U., Mal, N.K., Manna, A., and Bhaumi, A., *Ind. Eng. Chem. Res.* **42**, 3012 (2003).
128. Liu, S.C., Wang, W.X., and Chen, S.Y., *Cuihua Xuebao* **17**, 497 (1996).
129. Wang, K.X., Hao, Z.Y., Deng, J.C., Liu, M.L., and Lu, G.H., *Mater. Lett.* **28**, 277 (1996).
130. van de Loosdrecht, J., van der Kraan, A.M., van Dillen, A.J., and Geus, J.W., *Catal. Lett.* **41**, 27 (1996).
131. Wu, Q., Li, X., and Zhang, M.Z., *Cuihua Xuebao* **18**, 338 (1997).
132. Herreyre, S., Gadelle, P., Moral, P., and Millet, J.M.M., *J. Phys. Chem. Solids* **58**, 1539 (1997).
133. Boellaard, E., van de Scheur, F.T., van der Kraan, A.M., and Geus, J.W., *Appl. Catal. A* **171**, 333 (1998).
134. Lin, L.W., Yang, W.S., Jia, J.F., Xu, Z.S., Zhang, T., Fan, Y.N., Kou, K., and Shen, J.Y., *Sci. China, Ser. B* **42**, 571 (1999).

135. Zeifert, B.H., Salmones, J., Hernández, J.A., Reynoso, R., Nava, N., Cabañas-Moreno, J.G., and Aguilar-Ríos, G., *Catal. Lett.* **63**, 161 (1999).
136. Jia, J.F., Shen, J.Y., Lin, L.W., Xu, Z.S., Zhang, T., and Liang, D.B., *J. Mol. Catal. A* **138**, 177 (1999).
137. Watanabe, Y., Banno, K., Nagai, Y., Matsuoka, Y., Kimura, M., Sugiura, M., *in* "Clays for our future" Proceedings of the 11th International Clay Conference (H. Kodama, A.R. Mermut and J.K. Torrance, Eds.), p. 173, 1999.
138. Teng, R.H., Sun, S.J., Liu, S., Liu, X., Ma, R.Z., and Liu, T., *Trans. Nonferrous Met. Soc. China* **9**, 562 (1999).
139. Debeila, M.A., Pollak, H., Coville, N.J., and Motjope, T.R., *Hyp. Interact.* **120**, 757 (1999).
140. Zeifert, B.H., Salmones, J., Hernández, J.A., Reynoso, R., Nava, N., Cabañas-Moreno, J.G., and Aguilar-Ríos, G., *Mater. Lett.* **43**, 244 (2000).
141. Jiang, M., Koizumi, N., and Yamada, M., *J. Phys. Chem. B* **104**, 763 (2000).
142. Salmones, J., Zeifert, B.H., Hernández, J.A., Reynoso, R., Nava, N., Cabañas-Moreno, J.G., and Aguilar-Ríos, G., *Stud. Surf. Sci. Catal.* **130**, 2255 (2000).
143. Zeifert, B.H., Salmones, J., Hernández, J.A., Reynoso, R., Nava, N., Reguera-Ruiz, E., Cabañas-Moreno, J.G., and Aguilar-Ríos, G., *J. Radioanal. Nucl. Chem.* **245**, 637 (2000).
144. Watanabe, Y., Banno, K., and Sugiura, M., *Appl. Clay Sci.* **16**, 59 (2000).
145. Boellaard, E., van der Kraan, A.M., and Geus, J.W., *Appl. Catal. A* **224**, 1 (2002).
146. Rachmady, W., and Vannice, M.A., *J. Catal.* **209**, 87 (2002).
147. Coquay, P., Vandenberghe, R.E., De Grave, E., Fonseca, A., Piedigrosso, P., and Nagy, J.B., *J. Appl. Phys.* **92**, 1286 (2002).
148. Shah, N., Pattanaik, S., Huggins, F.E., Panjala, D., and Huffman, G.P., *Fuel Process. Technol.* **83**, 163 (2003).
149. Schmauke, T., Menzel, M., and Roduner, E., *J. Mol. Catal. A* **194**, 211 (2003).
150. Hobson, M.C. Jr., Goresh, S.L., and Khare, G.P., *J. Catal.* **142**, 641 (1993).
151. Sales, E.A., Jove, J., Nectoux, F., Bozon-Verduraz, F., and Mendes, M.J., *Hyp. Interact.* **112**, 13 (1998).
152. Cortright, R.D., and Dumesic, J.A., *J. Catal.* **148**, 771 (1994).
153. Alcala, R., Shabaker, J.W., Huber, G.W., Sanchez-Castillo, M.A., and Dumesic, J.A., *J. Phys. Chem.* **109**, 2074 (2005).
154. Stievano, L., Wagner, F.E., Calogero, S., Recchia, S., Dossi, C., and Psaro, R., *Stud. Surf. Sci. Catal.* **130**, 3903 (2000).
155. Margitfalvi, J.L., Borbáth, I., Hegedus, M., Szegedi, A., Lázár, K., Gobölös, S., and Kristyán, S., *Catal. Today* **73**, 343 (2002).
156. Margitfalvi, J.L., Borbáth, I., Vankó, Gy., Hegedus, M., Gobölös, S., and Vértes, A., *J. Mol. Catal. A* **162**, 209 (2000).
157. Menzel, M., Mehner, H.W., Mönnich, I., and Berndt, H., *Hyp. Interact.* **126**, 89 (2000).
158. Millet, J.M.M., Toyir, J., Didillon, B., Candy, J.P., Nedez, C., and Basset, J.M., *Hyp. Interact.* **108**, 477 (1997).
159. Charlton, J.S., and Cordey-Hayes, M., *J. Less Common Metals* **20**, 105 (1970).
160. Berndt, H., Mönnich, I., Lücke, B., and Menzel, M., *Appl. Catal. B* **30**, 111 (2001).
161. Chaudhari, K., Das, T.K., Rajmohanan, P.R., Lazar, K., Sivasanker, S., and Chandwadkar, M., *J. Catal.* **183**, 281 (1999).
162. Friedl, J., Wagner, F.E., Nkosi, B., Towert, M., Coville, N.J., Adams, M.D., and Hutchings, G.J., *Hyp. Interact.* **69**, 767 (1991).
163. Shah, P., Ramaswamy, A.V., Lazar, K., and Ramaswamy, V., *Appl. Catal. A* **273**, 239 (2004).
164. Kobayashi, Y., Nasu, S., Tsubota, S., and Haruta, M., *Hyp. Interact.* **126**, 95 (2000).
165. Goossens, A., Crajé, M.W.J., van der Kraan, A.M., Zwijnenburg, A., Makkee, M., Moulijn, J.A., Grisel, R.J.H., Nieuwenhuys, B.E., and de Jongh, L.J., *Hyp. Interact.* **139/140**, 59 (2002).
166. Goossens, A., Crajé, M.W.J., van der Kraan, A.M., Zwijnenburg, A., Makkee, M., Moulijn, J.A., and de Jongh, L.J., *Catal. Today* **72**, 59 (2002).
167. Roberts, L.D., Pomerance, H., Thomson, J.O., and Dam, C.F., *BAPS* **7**, 565 (1962).
168. Shenoy, G.K., *Rev. Mod. Phys.* **36**, 339 (1964).

169. Faltens, M.O., and Shirley, D.A., *Chem. Phys.* **53**, 4249 (1970).
170. Daniells, S.T., Overweg, A.R., Makkee, M., and Moulijn, J.A., *J. Catal.* **230**, 52 (2005).
171. Berry, F.J., *Hyp. Interact.* **111**, 35 (1998).
172. Villa, P.L., Carbucicchio, M., Pessot, R., and Rateo, M., *Hyp. Interact.* **116**, 137 (1998).
173. Zanthoff, H.W., Grünert, W., Buchholz, S., Heber, M., Stievano, L., Wagner, F.E., and Wolf, G.U., *J. Mol. Catal. A* **162**, 443 (2000).
174. Baca, M., and Millet, J.M.M., *Appl. Catal. A* **279**, 67 (2005).
175. Millet, J.M.M., Roussel, H., Pigamo, A., Dubois, J.L., and Jumas, J.C., *Appl. Catal. A* **232**, 77 (2002).
176. Morozova, N.I., Kulakova, I.I., Afanasov, M.I., and Fabrichnyi, P.B., *Kinet. Catal.* **46**, 380 (2005).
177. Stievano, L., *Hyp. Interact.* **126**, 101 (2000).
178. Stievano, L., Calogero, S., Wagner, F.E., Galvagno, S., and Milone, C., *J. Phys. Chem. B* **103**, 9545 (1999).
179. Shen, J.Y., Guang, B., Xia, Y.F., and Chen, Y., *Wuji Huaxue Xuebao* **11**, 429 (1995).
180. Zhang, H.L., Shen, J.Y., and Ge, X., *J. Solid State Chem.* **117**, 127 (1995).
181. Xu, J., and Bartholomew, C.H., *J. Phys. Chem. B* **109**, 2392 (2005).
182. Benaichouba, B., Bussiere, P., Coudurier, C., and Vedrine, J.C., *Hyp. Interact.* **69**, 743 (1991).
183. Benaichouba, B., Bussiere, P., and Vedrine, J.C., *Appl. Catal. A* **130**, 31 (1995).
184. Zhang, H.L., Shen, J.Y., and Ge, X., *J. Solid State Chem.* **117**, 127 (1995).
185. Mitov, I.G., Dotcheva, D., Cherkezova-Zheleva, Z., and Mitrov, V.I., *NATO Sci. Ser., Ser. C* **546**, 383 (2000).
186. Mitov, I.G., and Andreev, A.A., *Bulg. Chem. Commun.* **30**, 1 (1998).
187. Manish, B.V., and Delgass, N.W., *J. Catal.* **187**, 506 (1999).
188. van Berge, P.J., and Everson, R.C., *Stud. Surf. Sci. Catal.* **107**, 207 (1997).
189. Iglesia, E., Soled, S.L., Fiato, R.A., and Via, G.H., *J. Catal.* **143**, 345 (1993).
190. Millet, J.M.M., Ponceblanc, H., Coudurier, G., Herrmann, J.M., and Vedrine, J.C., *J. Catal.* **142**, 381 (1993).
191. Margitfalvi, J.L., Vankó, G., Borbath, I., Tompos, A., and Vértes, A., *J. Catal.* **190**, 474 (2000).
192. Margitfalvi, J.L., Borbáth, I., Lázár, K., Tfirst, E., Szegedi, A., Hegedus, M., and Gobölös, S., *J. Catal.* **203**, 94 (2001).
193. Lazar, K., Rhodes, W.D., Borbath, I., Hegedüs, M., and Margitfalvi, J.L., *Hyp. Interact.* **139/140**, 87 (2002).
194. Bouwkamp-Wijnoltz, A.L., Visscher, W., van Veen, J.A.R., Boellaard, E., van der Kraan, A.M., and Tang, S.C., *J. Phys. Chem. B* **106**, 12993 (2002).
195. Bartholomew, C.H., and Boudart, M., *J. Catal.* **29**, 278 (1973).
196. Overweg, A.R., Crajé, M.W.J., Arends, I.C.W., and van der Kraan, A.M., *Hyp. Interact.* **141/142**, 391 (2002).
197. Bodker, F., Chorkendorff, S., and Morup, S., *Z. Phys. D* **40**, 152 (1997).
198. Wang, J., Zhu, Z.L., and Li, C.L., *J. Mol. Catal. A* **139**, 31 (1999).
199. Alvarez, A.M., Marchetti, S.G., Cagnoli, M.V., Bengoa, J.F., Mercader, R.C., and Yeramian, A.A., *Appl. Surf. Sci.* **165**, 100 (2000).
200. Burger, K., Vertes, A., Dekany, I., Szekeres, M., Homonnay, Z., Nemes-Vetessy, Z., and Buzas, N., *Colloid Polym. Sci.* **275**, 587 (1997).
201. Pol'shina, A.E., Puziy, A.M., Pol'shin, E.V., Faragher, R.G.A., and Mikhalovsky, S.V., "Fundamentals of Adsorption, Proceedings of the International Conference on Fundamentals of Adsorption." p. 741 5th, Kluwer publisher, Boston, 1995.
202. Verckhusen, B.M., *Chem. Commun.* **97**, 97 (2002).
203. Millet, J.M.M., Knözinger, H., and Bonville, P., *J. Phys. Chem. B.* **110**, 16003 (2006).
204. Bachari, K., Millet, J.M.M, Bonville, P., Figueras, F., and Cherifi, O., *J. Catal*. in press (2007).
205. Maltsev, Yu., Maltsev, S., Monzel, M., Rogozev, B., and Silvestrov, A., *Hyp. Interact.* **156/157**, 27 (2004).
206. Mashlan, M., Yevdokimov, V., Pechousk, J., Zboril, R., and Kholmetskii, A., *Hyp. Interact.* **156/157**, 15 (2004).
207. Guenzburger, D., Ellis, D.E., and Zeng, Z., *Hyp. Interact.* **113**, 25 (1998).

208. Paulsen, H., and Trautwein, A.X., *Top. Curr. Chem.* **235**, 197 (2004).
209. McCammon, C.A., Chaskar, V., and Richards, G.G., *Meas. Sci. Technol.* **2**, 657 (1991).
210. McCammon, C.A., *Hyp. Interact.* **92**, 1235 (1994).
211. de Souza, P.A. Jr., *Hyp. Interact.* **113**, 383 (1998).
212. de Souza, P.A. Jr., Garg, R.V., and Garg, K., *Hyp. Interact.* **112**, 275 (1998).
213. Rancourt, D.G., *Hyp. Interact.* **117**, 3 (1998).
214. Smith, P.R., Cashoin, J.D., and Brown, L.J., *Hyp. Interact.* **71**, 1503 (1992).
215. Gerdau, E., and DeWaard, H., *Hyp. Interact.* **123/124** (1999).
216. Rancourt, D., and Klingelhöfer, G., Fourth Seeheim Workshop on Mössbauer Spectroscopy Abstracts, p. 129, 1994.
217. Gerdau, E., van Bürck, U., and Rüffer, R., *Hyp. Interact.* **123/124**, 3 (1999).
218. Leupold, O., *Hyp. Interact.* **144/145**, 21 (2002).
219. Leupold, O., Chumakov, A.I., Alp, E.E., Sturhahn, W., and Baron, A.Q.R., *Hyp. Interact.* **124/124**, 611 (1999).
220. Grünsteudel, H.F., Haas, M., Leupold, O., Mandon, D., Matzanke, B.F., Meyer-Klaucke, W., Paulsen, H., Realo, E., Rüter, H.D., Trautwein, A.X., Weiss, R., and Winkler, H., *Inorg. Chim. Acta* **275/276**, 334 (1998).
221. Lübbers, R., Wortmann, G., and Grünsteudel, H.F., *Hyp. Interact.* **123/124**, 529 (1999).
222. Leupold, O., and Winckler, H., *Hyp. Interact.* **123/124**, 571 (1999).
223. Singwi, K.S., and Sjölander, A., *Phys. Rev.* **120**, 1093 (1960).
224. Rüffer, R., and Chumakov, A.I., *Hyp. Interact.* **128**, 255 (2000).
225. Chumakov, A.I., Rüffer, R., Baron, A.Q.R., Grünsteudel, H., Grünsteudel, H.F., and Kohn, V.G., *Phys. Rev. B* **56**, 10758 (1997).
226. Chumakov, A.I., Rüffer, R., Baron, A.Q.R., Grünsteudel, H., and Grünsteudel, H.F., *Phys. Rev. B* **54**, 9596 (1996).
227. Vanko, G., Bottyan, L., Nagy, D.L., Szilagyi, E., and Vertes, A., *J. Rad. Nucl. Chem.* **246**, 97 (2000).
228. Nomura, K., Rykov, A., Mitsui, T., Yoda, Y., Kobayashi, Y., Seto, M., and Sawada, T., *J. Rad. Nucl. Chem.* **255**, 187 (2003).